Optimisation of Microwindow Positioning for the Detection of Cloud in MIPAS Spectra

Harry Desmond

Nuffield Bursary Project
Department of Atmospheric, Oceanic and Planetary Physics
Oxford University

Summer 2007

Abstract:

The aim of this project was to optimise the methods for detecting cloud in MIPAS spectra. MIPAS is a spectrometer on board the European Space Agency's Envisat. If not properly identified, cloud-filled spectra can lead to serious misinterpretations of data. The project focused on the positioning of the microwindows (MW, regions of the electromagnetic spectrum) used to calculate the Cloud Index. Two distinct criteria were used.

a) The strength of the correlation of the Cloud Index (the ratio of the mean observed radiance within two MWs) with the Cloud Effective Fraction (the geometric fraction of the field of view that is filled by cloud multiplied by the optical absorption of the cloud). A 11.7 % increase in correlation strength on the microwindows in current usage was demonstrated through alteration of MW positioning. A further 2.13% improvement was achieved through iterative methods.

b) The extent of the separation of the clear from cloudy spectra. Greater separation indicates reduced probability of accidental discarding of clear spectra. Three different methods were explored, each adopting distinct measures of separation. Two revealed MWs receiving a more favourable assessment than the operational MWs, whilst the third, deemed most reliable, showed the current MWs to exhibit a 28.3% greater separation than the best alternative MW pair tested in this paper.

Keywords: MIPAS, microwindows, cloud detection

Contents

1. MIPAS Background

MIPAS, the Michelson Interferometer For Passive Atmospheric Sounding, is one of the core instruments on board the European Space Agency's Envisat. Launched in March 2002 [1], this is a sun-synchronous Earth observation satellite in a polar orbit at an altitude of 800 km. [2] The orbital inclination of 98.54 degrees, coupled with the period of 100.6 minutes, permits complete global coverage [2] during both the day and the night [3]. MIPAS itself is located towards the rear of the satellite, and can conduct observations in one of two directions: antiparallel to the direction of the motion of the satellite, and perpendicular to the flight direction away from the sun. The former permits freedom of line-of-sight selection over 35 degrees, and the latter 30 [4] - both viewing modes enable the projection of a 3 x 30 km field-of-view onto the observed atmospheric region [5].

The data obtainable from MIPAS are infrared spectra. The instrument itself records the intensity of radiation (measured as the quantity radiance, with dimensions $nW / cm^2 \text{ sr } cm^{-1}$) as a function of time; this signal is converted into a spectrum, which represents intensity of light as a function of frequency of that light, by suitable ground processing. The backdrop for MIPAS measurements is space (it is therefore termed a limb-viewing spectrometer, as opposed to nadir-viewers which use the Earth's surface as a backdrop), and thus the received radiation originates from gas molecule emission in the Earth's atmosphere. Gas emission lines are formed in the visible region of the spectrum by quantized electronic transitions within atoms, but in the infrared, where photon energies are considerably lower, they originate from excitation of molecular vibration and rotation states. Due to variation in atomic arrangement, every molecule absorbs energy of a different frequency to attain a higher vibrational mode, and hence each molecule has lines at characteristic frequencies. This allows the concentration of each molecule to be identified from spectra by examination of the frequency and intensity of the emission signatures. MIPAS was designed in particular for the study of ozone (O_3), water (H_2O), nitric acid (HNO_3), methane (CH_4), nitrogen dioxide (NO_2) and nitrous oxide (N_2O) [2]. The raw spectra are termed level 1B data, whilst level 2 processing describes the subsequent generation of atmospheric concentration profiles of these major gases, from spectral information [4]. The ultimate objective is the improvement of both current climatological models and of stratospheric reaction mechanisms [6], in particular those documenting the relationship between CFCs and ozone in the stratosphere, although observations also have prominent application in the field of weather forecasting [4]. Temperature and pressure profiles through the atmosphere are also attainable from CO_2 emission lines. These parameters affect the observed gas concentrations, and hence such profiles permit compensation. [6,7].

In terms of instrument operation, MIPAS is classed as a Fourier Transform Spectrometer [6], the principles of which merit explanation. The primary functional component is a Michelson Interferometer, which typically consists of a light source (which, in the case of MIPAS, is infrared radiation emitted by the Earth's atmosphere), a beamsplitter used to fragment incident light into two separate channels of equal power [4], two mirrors, and a light-sensitive detector. Its operation proceeds as follows. Light from the source is first collimated (all rays are aligned along a common axis) and then shone on the beamsplitter, which permits passage to one half of the incident light, whilst reflecting the other half so that it follows a path perpendicular to its counterpart. The mirrors, situated at a predefined distance along the two paths, reflect the beams back towards the beamsplitter, where they interfere. Interference, the result of wave superposition, is the process whereby the amplitude of two waves sum vectorially to give a resultant amplitude. A minimum resultant amplitude is generated from waves superposing in antiphase (their associated vectors are antiparallel), whilst an exaggerated amplitude is formed by in phase superposition. The intensity of the light spot produced (and hence its apparent brightness), which is proportional to the square of the resultant amplitude, will therefore be maximised. Due to the constancy of the speed of light, the former (termed destructive interference) will occur when the difference in length between the paths from the beamsplitter to each mirror is $n*\lambda + \lambda / 2$, where n is an integer and λ the wavelength of the light in question, and the latter (constructive interference) when the path difference is $n*\lambda$. Thus both the wavelength and radiance of

the incident light may be determined by studying the interference pattern.

Fourier Transform Spectrometers, however, modify certain aspects of the above account. Foremost among these is the fact that one (or, in the case of MIPAS, both) of the mirrors are not fixed. The mobile mirrors are scanned parallel to the light path (for MIPAS, over a distance of 100 nm at a speed of 0.25 nm/s). In addition, the interference pattern observed at the beamsplitter is used to modulate a cosine wave. This modulated output is sampled at high frequency and the result recorded and processed to form the desired spectrum. Perturbations caused by orbital altitude deviations can be rectified by the scanning mirrors, which also facilitate selection of the line-of-sight (that is, the path through which the input radiation will have travelled) [2].

MIPAS operates in the infrared region of the electromagnetic spectrum - the spectral range is 685 - 2410 cm^{-1} [5], but is split up for convenience into five distinct bands [6]. The A band (685 - 970 cm^{-1}) will be the prime concern of this investigation due to past success in Cloud Index formulation (a concept to be explained in detail shortly) in this area. The resolution of the instrument is 0.025 cm^{-1} throughout its spectral range [5] (i.e. if a radiance value is recorded at a particular frequency, the consecutive measurement will relate to radiation with frequency 0.025 cm^{-1} greater). This is determined by the inverse of the maximum optical path difference between the interferometer mirrors (40 cm). Spectra were recorded by MIPAS at 17 altitudes (6km through 42km above the Earth's surface in 3km steps, in addition to 47km, 52km, 60km, and 68km [5]), although those of interest in this project will be 6km, 9km, 12km, 15km, 18km, and 21km. In practice, these are the last 6 altitudes to be scanned during each sweep, as MIPAS starts at 68 km and proceeds downwards. 4.5 seconds are required at each altitude for the generation of a spectrum, and consecutive measurements at a particular altitude are separated by 500 km [2].

Although intended to run at optimal performance for a five year period [6], MIPAS began experiencing problems in March 2004; instrument failure was becoming common due to irregular motion of the mirrors. This was rectified in January 2005 by the reduction of the maximum mirror displacement to 40% of its initial value. Thus the maximum distance between the mirrors fell from 40 to 16.4 cm, improving the resolution to 1 / 16.4 = 0.0625 (representing a 2.5 fold reduction in spectral information content), although this was offset by a 3 - 4 fold increase in the spectral range. The shorter measurement time of 1.8 seconds was exploited by the introduction of additional scanning altitudes in the troposphere and lower stratosphere, and precision was improved due to noise reduction accompanying the decreased resolution. Further disadvantages, however, included an increase in the computing time necessary to process a complete scan (by a factor of 5), and an overall increase in the noise associated with each spectral point [1]. The duty cycle of the instrument (that is, the percentage of the time during which it actively takes measurements) fell to 35%, although a duty cycle of 80% has now been resumed [3].

2. Motivation for cloud detection in MIPAS spectra

It should be noted at this juncture that of the factors currently resulting in a severe reduction of spectral information content, one of the most prominent is cloud. Indeed, the presence of cloud is often quoted as a major limitation of infrared limb viewing instruments such as MIPAS [4]. General information regarding cloud formation, type and location will be presented in the next section. This section aims to document the purpose of cloud detection, not only as a means of discarding spectra which are believed to be cloud contaminated, but also for the study of clouds for their own sake.

Fundamentally, clouds create a continuum-like increase in radiance across a wide range of frequencies. One might expect that the contribution of clouds to a spectrum would merely be an exaggeration of the emission lines of water molecules (since clouds consist solely of water), but this is not the case. The water molecules within a cloud are in the solid or liquid phase, and hence the relatively strong intermolecular bonds (hydrogen bonds and dispersion forces) inhibit molecular vibration and rotation, with the result that the emission line is much broadened. The scattering of

radiation from clouds can also result in the detection of radiation originating from outside the MIPAS field of view. In short, much useful information in cloud infected regions is lost or skewed. The following diagrams illustrate the contribution of cloud to observed radiance.

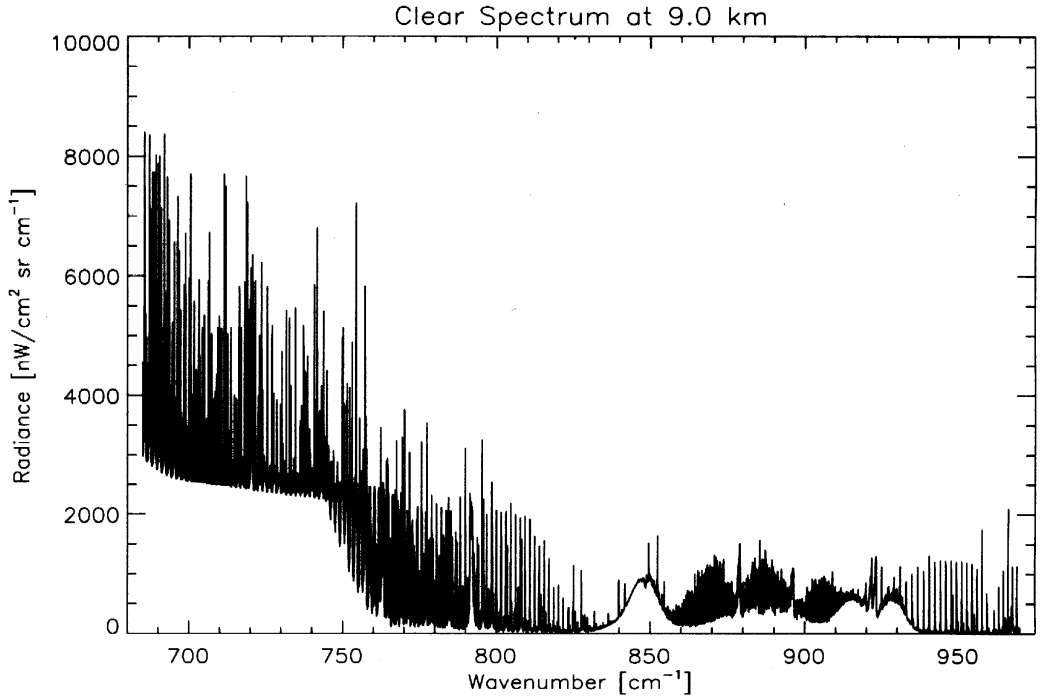

Figure 1: A typical clear (cloudless) spectrum modelled at an altitude of 9.0 km

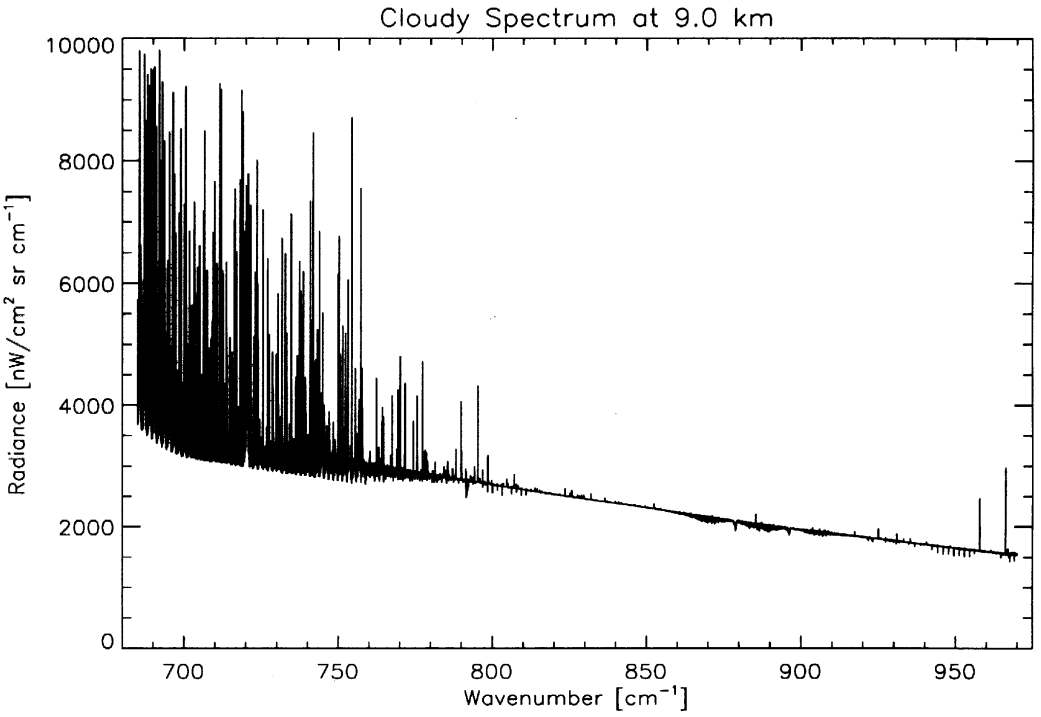

Figure 2: A typical spectrum modelled in the presence of thick cloud, at 9.0 km

However, with no method for the immediate identification of such cloudy spectra, the radiance values within cloud-infected regions would be given as much weight as those without, generating false information. Hence the development of a reliable cloud detection method is imperative, with the aim of discarding spectra that contain excessive quantities of cloud.

The impact of clouds extends far beyond a mere annoyance, however: clouds are an integral part of every meteorological system. Heat is evolved when they form (due to the exothermic nature of the creation of intermolecular forces), whilst their evaporation is endothermic. However, the overall effect of clouds on the temperature balance of the Earth is more complex: they absorb both solar radiation and infrared radiation from the Earth's surface, and subsequently re-radiate the energy in all directions. Absorption and emission of solar radiation tends to cool the Earth, as a reduced proportion of the energy content of this radiation reaches the surface. Similar processes for infrared radiation warm the Earth, as some of this energy (which, without cloud, would have been transmitted into space) is now redirected towards the Earth's surface [2]. The relative prevalence of each of these factors is determined in large part by the location of the cloud within the atmosphere, with the propensity of lower clouds being to cool the planet and vice versa. This is because lower clouds tend to have a higher reflectivity to solar radiation than high clouds, and also are warmer and so re-emit more infrared radiation into space. The net global effect of cloud is currently believed to be a cooling of approximately 17 W / m^2 (that is, on average, clouds cause the deprivation of 17 joules of energy to each square metre of the Earth's surface every second). Current models imply that without clouds, the surface of the planet would be 10 - 15˚C warmer [2]. Additional effects of clouds within the atmosphere include the precipitation of water vapour into liquid or solid form (the process by which this occurs will be detailed later), and a significant reduction in the rate of temperature decrease at higher altitudes. The latter is linked with the exothermic nature of cloud formation - at higher altitudes water is more likely to condense into clouds, releasing heat [2]. That said, there are numerous uncertainties in the mechanisms whereby clouds exact their effect. For example, the relation between cloud radiative effects and climate change, and the effect of cirrus on climate sensitivity, are both poorly understood [2]. Cloud study is therefore vital for furthering our models of the radiative budget of the Earth, as well as specific atmospheric chemical pathways. The first step towards cloud study must surely be their detection.

3. Cloud Background

The significance of cloud not only to MIPAS spectra but to the atmosphere in general merits elucidation of their composition, formation and categorisation. Technically, a cloud is 'a visible aggregate of minute suspended particles of water or ice in the atmosphere' (WMO, 1975, from [2]). However, clouds are not static, rather they represent dynamic systems: constituent ice or water particles evaporate whilst new ones take their place. They form when the air becomes supersaturated with water vapour, necessitating its condensation into liquid or solid form. This process occurs as the air cools, either through expansion at high altitude, emission of radiation, or conductive energy loss to an adjacent, cooler air mass [2]. However, simple supersaturation is not enough - in ideally clean air, a temperature of - 40˚C coupled with a water vapour humidity of several hundred percent would be necessary to initiate significant cloud formation [8]. Also required are Cloud Condensation Nuclei - particles of diameter approximately 1 micron (10^{-6} m) which facilitate the condensation process. Although the exact constituents of such nuclei are varied in nature (typical forms include sea salts [comprising 20% of the total], combustion products [40%] and soil particles [20%] [9]), those most effective in the generation of cloud are hygroscopic, and thus retain water [2]. (Nuclei-dependant condensation is termed heterogeneous, whilst nuclei-independent condensation, insignificant due to its extreme rarity, is termed homogeneous [8].) The accumulation of water on the nuclei forms a haze droplet, which becomes a cloud droplet after attaining a diameter of approximately 10 microns [8]. Although these general formation processes are applicable to ice clouds also, some details are

different, notably the requisite nuclei are termed 'Ice Nuclei' [8]. Different forms of such nuclei can initiate the formation of ice clouds at different temperatures. The most effective is ice, which, by acting as a catalyst for its own formation, permits nucleation at the freezing point of water. Ice nuclei can also be formed through stochastic fluctuations in the molecular arrangement of water, causing it to adopt a structure resembling ice [8].

The forms of cloud are many and varied. When the field of cloud study was nascent, four general types were identified: cumulus, stratus, cirrus and nimbus. However, in subsequent decades, clouds were discovered which did not conform to just one of these types, and hence the categories were often combined for a more complete description. Additional detail was provided by the appendage of a phrase denoting the typical altitude at which a particular cloud is found, or its specific mechanism of formation. Today, ten distinct cloud types are widely recognised. These are cirrus, cirrostratus, cirrocumulus, altostratus, altocumulus, nimbostratus, stratocumulus, stratus, cumulus and cumulonimbus. Each varies from its counterparts by the altitude of its situation in the atmosphere, the way it develops, and its visual appearance. Briefly, the first three are grouped as 'high clouds' (with altitude extending from 6 km to approximately 12 km); the following two are said to possess medium height (2 - 6 km), whilst the following three are termed low cloud. The final two are 'clouds with vertical development' - categorisation of these clouds into one of the three above classes is impractical as a single cloud may span a wide range of altitudes. A short description of each cloud type follows, based largely on data from [9]:

High Cloud:
Cirrus - white, wispy, often fibrous, sufficiently translucent for sky to be observed through them. The most common cloud type (30% of the Earth's surface may be covered by cirrus at any one time [2]).
Cirrocumulus - Semi-transparent, often assume the shape of ripples or scales.
Cirrostratus - thin, uniform, white/bluish. Form phenomena such as a halo around the sun, false sun and moon, and a horizontal disk passing through the sun.

Medium Height:
Altostratus - grey/bluish, covers entire sky. Sometimes possible to observe the sun and moon through them, although often opaque.
Altocumulus - lightly coloured, appear as ripples or delicate puffs through which the sky is visible. Sometimes fuse to give a thin continuous mantle. Approximately 0.3 km thick.

Low Cloud:
Stratocumulus - similar in structural development to altocumulus, but at lower altitude.
Stratus - grey, sometimes nearly uniform, yet sometimes tattered in the lowermost part to form descending irregular shreds. Presents significant difficulties to aviators due to its low altitude and opacity.
Nimbostratus - Resemble stratus, but thicker and more translucent. Typically bear rain.

Clouds with Vertical Development:
Cumulus - dense, predominantly white but with a flat and darkened base. Vertical extension up to 6-7 km has been observed. Individual clouds are separated by considerable gaps.
Cumulonimbus - similar to cumulus in lower parts, although top appears horizontal and resembles cirrus. Can dissociate at lower levels to form layers of altostratus and altocumulus, and, for this reason, are often referred to as 'cloud factories'.

The alterations effected by particular cloud types upon the generalised formation account presented above has received much attention, although details are still disputed. The general consensus is that cirrus is formed by a warm front being forced over a cold front (inducing condensation), whilst cumulus is formed by convective air motion, often on mountainsides [8]. Stratus, on the other hand, is generated by advection of warm moist air, particularly of marine origin (that is, larger scale motion of

air in the horizontal direction). Other types may be formed by a combination of these processes, although, in general, any type may form at any altitude by the meeting and subsequent interaction of two air masses of differing thermodynamic properties [9].

4. Cloud Detection Methodology

Clouds are detected in MIPAS spectra by virtue of their effect of increasing the observed radiance. The simplest detection method is therefore to define a radiance threshold at a particular frequency (whose radiance value should be determined through careful analysis of numerous sample spectra containing various quantities of cloud). Spectra with a radiance value above this threshold at that particular frequency are discarded as containing too much cloud. It is important to note, however, that in all discussions of thresholds, its value, being as it is defined by the user, will vary considerably depending on the user's intent. For example, if one wishes to discount only very thick cloud (which increases the radiance by a large amount), the threshold will be set to a higher value than if it is desirable for thinner cloud-containing spectra to be discarded also. For MIPAS spectra, this threshold is often set, in the region of 960.7 cm^{-1}, at a radiance value of 100 nW / cm^2 sr cm^{-1} for the detection of very thin cloud at an altitude of approximately 9 km [2]. It can be seen that this threshold would identify figure 2 as being cloud-contaminated, but not figure 1.

An improved technique involves a radiance ratio (termed the Cloud Index), and will be the prime concern of this report. The necessity for improvement upon the simple threshold technique is derived from the fact that the result is prone to pressure and temperature variations. For example, a higher temperature may push the radiance over the threshold even if there is no cloud, introducing significant uncertainty into the outcome. The Cloud Index (CI) is calculated as the ratio of the mean radiances in two regions of the MIPAS spectrum, called microwindows (MWs - hence CI = MW1 / MW2). Both of these radiances will be affected approximately equally by temperature and pressure, and hence their ratio will remain constant. It can be seen from figures 1 and 2 of clear and cloudy A band spectra that only a certain region is affected by cloud (from approximately 750 cm^{-1} onwards). The principle behind the Cloud Index is that the first MW, MW1, is selected in a region that is little changed by the presence of cloud, and the second, MW2, in a region that is significantly affected. Thus when cloud is present, the denominator is increased whilst the numerator remains roughly constant, and hence the CI value drops. As before, a threshold value is set according to the type of cloud that one wishes to exclude.

The pioneers of this method were Reinhold Spang and John Remedios of Leicester university, who suggested, based on data from CRISTA, a grating spectrometer [7], that optimal MW positions were as follows: MW1: 788 - 796 cm^{-1} (i.e. the numerator of the CI formula would be the mean radiance observed between these two boundaries) and MW2: 832 - 834. However, aspersions have been cast on the objective nature of their findings: it has been argued that insufficient data was analysed to form the basis of this conclusion, and comprehensive MW selection schemes were not applied, and hence the chosen positions cannot be considered optimum in any quantifiable sense. It is the objective of this project to validate the critics by locating more suitable MW positions. Spang and Remedios further concluded that the CI threshold, below which spectra would be disregarded due to cloud-contamination, should be set at 1.8 [2] (note that the CI is a ratio of two quantities with the same dimensions, and thus the CI itself is dimensionless).

The above discussion of CI is related solely to its use in the MIPAS A band (685 - 970 cm^{-1}), but it is worth noting that Cloud Indices have been developed in other bands also. It has been suggested, for example, that D band MWs may be useful as a means of validating results gleaned by A band MWs. This was hypothesised after the discovery of several cloud cases that were correctly identified by D band MWs, but not those situated in the A band. However, evidence was soon accrued which suggested that D band MWs were not suitable for cloud detection - for example, it was often found that the D band CI would report cloud at impossibly high altitudes, yet extremely thick cloud

within the MIPAS field of view was not consistently identified [2]. It seems probable, therefore, that the A band will remain the sole region of MW positioning, and hence this project will focus exclusively on it.

5. Optimisation of MW positioning through the maximisation of the strength of the correlation of the relationship between CI and the CEF

5.1 CI, CEF and RMSE calculation for the initial MWs

It is not immediately obvious what the criteria will be for judging a good combination of microwindow positions. Two will be explored in this paper. The first involves a new quantity, the Cloud Effective Fraction (CEF), which, fundamentally, is a single number providing a measure of not only the proportion of the MIPAS field of view that is filled with cloud, but also how optically thick that cloud is. Prior to an explanation of the derivation of the CEF, it is necessary to describe the MIPAS field of view (FOV) in more detail. Although often quoted (mainly for simplicity of expression) as a 30 x 3 km rectangle, it is actually a trapezoid of maximum height 4 km and maximum width 30 km. Each point within the FOV (called a tangent point) receives radiation from a cloud along a particular path. In this investigation, the vertical separation of each tangent point from its neighbours will be 10m, although this distance is not inherently implied by the instrument field-of-view and in practice any distance may be chosen. The peculiar shape of the FOV necessitates the formulation of a function (of the tangent point position) to account for which part of the FOV a particular light ray enters. This is called the convolution function. The distance between the Earth's surface and the centre of the FOV (which is 2 km above its lowest point) is designated as the tangent height, and is the nominal height at which MIPAS is scanning. The calculation of the CEF comprises several lines of reasoning, and equation formulations and reformulations: for ease of viewing, transitions will be indicated by numbering.

1. The radiance from each particular tangent point is multiplied by the corresponding convolution function value. The radiance received by the MIPAS instrument from a cloud in the FOV is the integral of this product, with respect to the tangent point, between the bottom of the FOV and the cloud top height [10]. This includes the radiance received from all parts of the FOV.

$$Cloud\,Radiance = \frac{\left(\int_{-d}^{z_{CTH}} L(z) * \psi(z)\,dz\right)}{\left(\int_{-d}^{d} \psi(z)\,dz\right)}$$

Where z is the position of the tangent point relative to the tangent height, L(z) is the radiance received at each particular tangent point, d is the distance between the tangent height and the bottom of the FOV (2km), z_{CTH} is the tangent point coincident with the cloud top, and ψ is the convolution function.

Notice also the denominator, which is the integral of the convolution function between the bottom and top of the FOV and serves to normalize the equation. The definition of the convolution function dictates that this integral should equal one, and therefore, after ensuring that this is the case, it may be disregarded in calculations.

2. For practical purposes, however, both integrals can be treated as a simple sum, since in reality there is a only discrete number of tangent points within the FOV. An equivalent expression would therefore be:

$$Cloud\,Radiance = \frac{(\sum_{-d}^{z_{CTH}} L(z) * \psi(z) dz)}{(\sum_{-d}^{d} \psi(z)\, dz)}$$

3. L(z) may also be expressed in a different manner. The radiance received from the cloud is measured by its extinction coefficient, which quantifies the extent to which the cloud scatters and absorbs radiation - a high extinction coefficient (k_{ext}) implies that radiation rapidly becomes extinct within it, through absorption. By definition, the k_{ext} is related to the received radiance by:

$$L(z) = e^{(-k_{ext} * E)} * B(T, V)$$

Where k_{ext} is the extinction coefficient, E is the length of the path through the cloud that the light has traversed, and B(T,V) is the Planck function corresponding to the cloud temperature T and wavenumber V. This final term serves to discount any radiative contribution from atmospheric scattering or gas molecules.

5. It now remains to formulate an expression for E based on known parameters. Figure 3 illustrates the key aspects of MIPAS' viewing geometry.

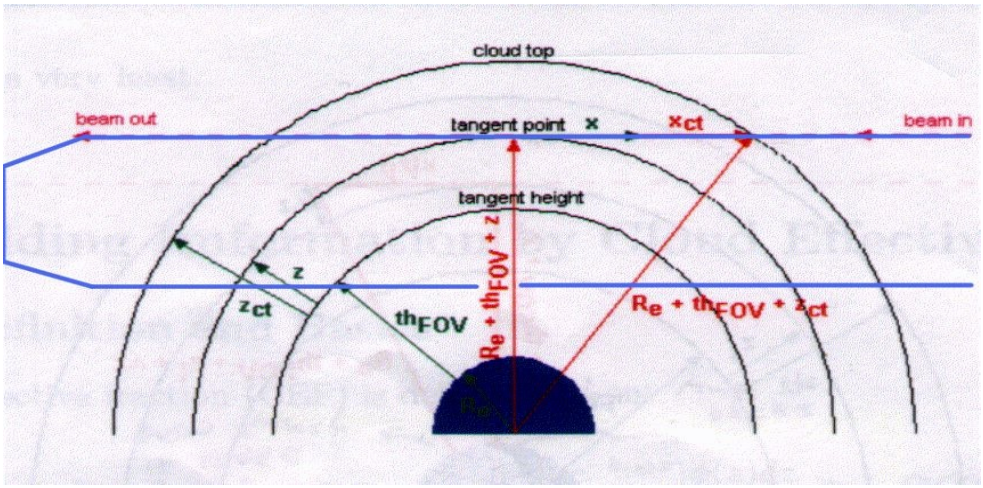

Figure 3: MIPAS viewing geometry in the presence of cloud, from source [10]. Blue lines indicate the extent of the field-of-view. Any light ray within these bounds is taken into consideration.

It can be seen that a triangle may be constructed with a right angle at the tangent point and two vertices at the centre of the Earth and the cloud top respectively. Pythagoras' theorem allows the path length to be expressed as:

$$E = \sqrt{(R_e + th_{FOV} + z_{CT}) - (R_e + th_{FOV} + z_i)}$$

Where R_e is the radius of the Earth, th_{FOV} is the tangent height of the FOV, z_{CT} is the z value of the cloud top height, and z_i is the z value for each tangent point between the bottom of the FOV and the cloud top.

6. The CEF, however, measures the optical blocking power of the cloud, which is one minus the

cloud's radiative contribution. L(z) from the cloud radiance formula is therefore replaced by 1 - L(Z), allowing the completion of the definition of the CEF. The Planck function term was neglected as a first approximation:

$$CEF = \frac{\left(\sum_{-d}^{z_{CTH}} \left(1 - e^{-k_{ext}E}\right) \psi(z)\, dz\right)}{\left(\sum_{-d}^{d} \psi(z) dz\right)} \quad [10]$$

For the CI to be a good measure of how much cloud there is in the field of view, it should correlate strongly with the CEF. If this is so then, after calculation of the CI for a particular spectrum, it would be possible to tell with high precision what the CEF of the spectrum is, and hence how much cloud there is in the FOV. Before experimenting with other MW positions, the correlation strength using the Spang/Remedios MWs (788 - 796 cm^{-1} and 832 - 834 cm^{-1}) will be assessed. The measure of correlation strength that will be used in this paper will be the root mean square error (RMSE), but evaluation of this requires the calculation of a best fit regression line.

It is necessary to digress at this point in order to explain the origin of the spectra that will be used. They are not actually recorded by MIPAS, rather they are generated by the Reference Forward Model (RFM). This is a line by line radiative transfer model used to simulate MIPAS spectra. In the presence of cloud, radiative transfer can be expressed as two distinct components: the non-scattering domain (that is, emission and absorption from the cloudless parts of the atmosphere), and the scattering domain (the radiative contribution of the cloud) [2]. In essence, the operation of forward models is the opposite of that of typical data retrieval schemes. The latter attempts to evaluate atmospheric parameters from observations (for example generating information regarding gas concentrations from MIPAS spectra), whilst the former uses defined parameters to predict what would be observed [11]. The RFM, upon definition of the tangent height, atmosphere type, cloud top height and cloud extinction coefficient, will generate a spectrum such as may be expected to be observed by MIPAS. In this paper, tangent heights of 6km, 9km, 12km, 15km, 18km and 21km will be used, along with the atmosphere types 'night', 'equatorial', 'winter', 'summer'. Four additional atmosphere types corresponding to statistical alterations applied to these four basic types will also be included. The extinction coefficient values will be restricted to 0.1, 0.01 and 0.001 km^{-1}, since below this the attenuation of the cloud would render the non-scattering domain insignificant (for all intents and purposes, such cloud could be neglected), yet cloud with a k_{ext} of greater than 0.1 cannot ordinarily be distinguished from cloud with a k_{ext} of 0.1, both cases assuming near-maximal conformation to a black body [10]. The cloud top heights will be at displacements of -2.0, -1.5, -1.0, -0.5, 0, 0.5, 1.0, 1.5 and 2.0 km from the tangent height - a cloud top height of -2.0 represents no cloud within the FOV, and hence an entirely clear spectrum may be obtained. The total number of atmospheric spectral types modelled, therefore, equals the total number of permutations of these four parameters; that is, 9 * 8 * 6 * 3 = 1296. A CI and CEF value is found for each of these spectra, and these constitute the data points for which the best line will be calculated.

Returning, then, to the methodology at hand, a program was written (in the IDL language) to calculate these 1296 CI and CEF values, the code of which is printed in appendix 4.1. Below is the diagram generated by the call to the IDL 'plot' procedure towards the end of the program.

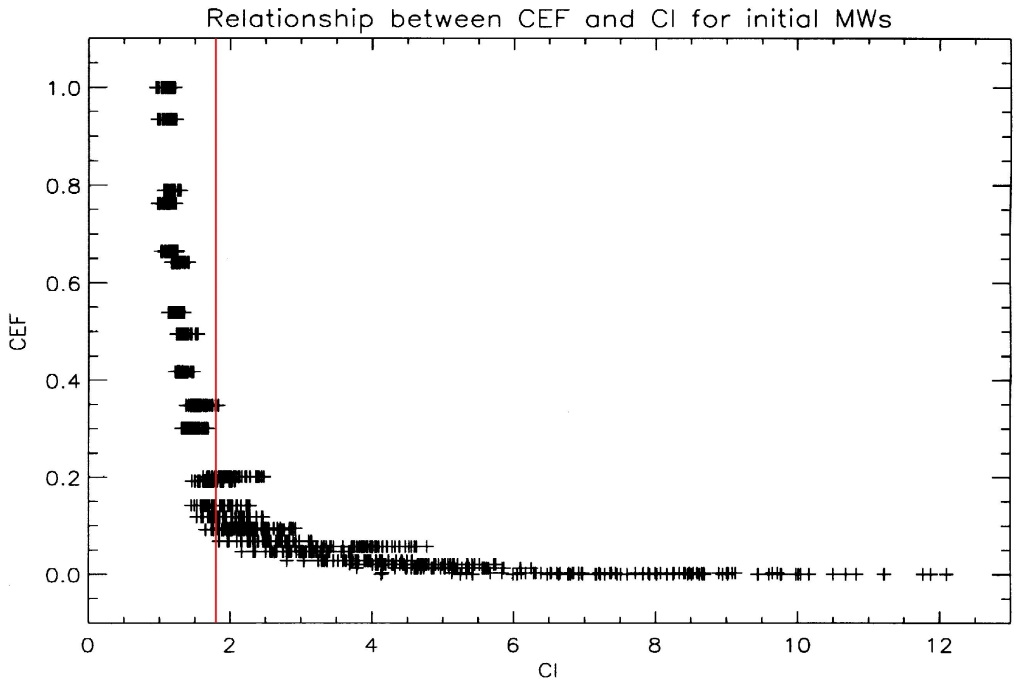

Figure 4: Plot of CI against CEF using the MW pair 788 - 796 with 832 - 834. Conventionally, spectra giving a CI lower than the threshold (1.8; indicated by the red line) are discarded as containing too much cloud.

Best fit lines must conform to a particular function, and the form of the function best representing this data is not obvious. Previous work conducted in this field [10] suggests that a fourth degree polynomial in $\log_{10}$(CI) may be suitable, although determination of the constants involved in such a fit is inconvenient. In addition, different atmospheric parameters were used in [10], and no attempt was made to optimize the function form through experimentation with other types. Alternative functions were therefore explored, and it was found that a plot of $\log_{10}$ (CI) against $\log_{10}$(CEF), shown in figure 2, exhibited strong linearity. Due to the relative ease of implementation of a linear best fit line (thanks in large part to IDL's purpose-built 'ladfit' procedure, using a least-squares minimization method) it was decided to adopt this form for future calculations. The best fit line would therefore be of the form $\log_{10}(CEF) = a + b * \log_{10}(CI)$ where a and b are real constants.

Note, however, that when the cloud top height is -2.0 (i.e. coincident with the bottom of the FOV, denoting clear spectra), the CEF is 0, and hence $\log_{10}$(CEF) is undefined. This was set at -2.5 for the purposes of this investigation, as it seemed to allow the clear spectral points to lie roughly on the best fit line. It may, however, have been better defined at a lower value, perhaps -3.0, to reduce its value below that obtained by the thinnest cloud case, which has a $\log_{10}$(CEF) of approximately -2.6. Note also that for a particular log(CEF) value, there are numerous log(CI) values. This is because the CEF depends, to a significant extent, only on the cloud's extinction coefficient and cloud top height (it varies to a very minor degree with tangent height). Thus there are only 3 * 9 = 27 distinct CEF values, corresponding to 27 horizontal 'rungs' of data points. The CI values, however, depend on all four atmospheric parameters (each affects the radiance values observed in all parts of the spectrum), and hence within each rung there are 8 * 6 = 48 distinct CI values. Finally, it is noticeable that the spread of CI values is less when the cloud is thicker (i.e. higher CEF value). This is because the radiative contribution of the cloud dominates the spectra, and hence variations in atmosphere type or tangent height make very little difference to spectral radiance.

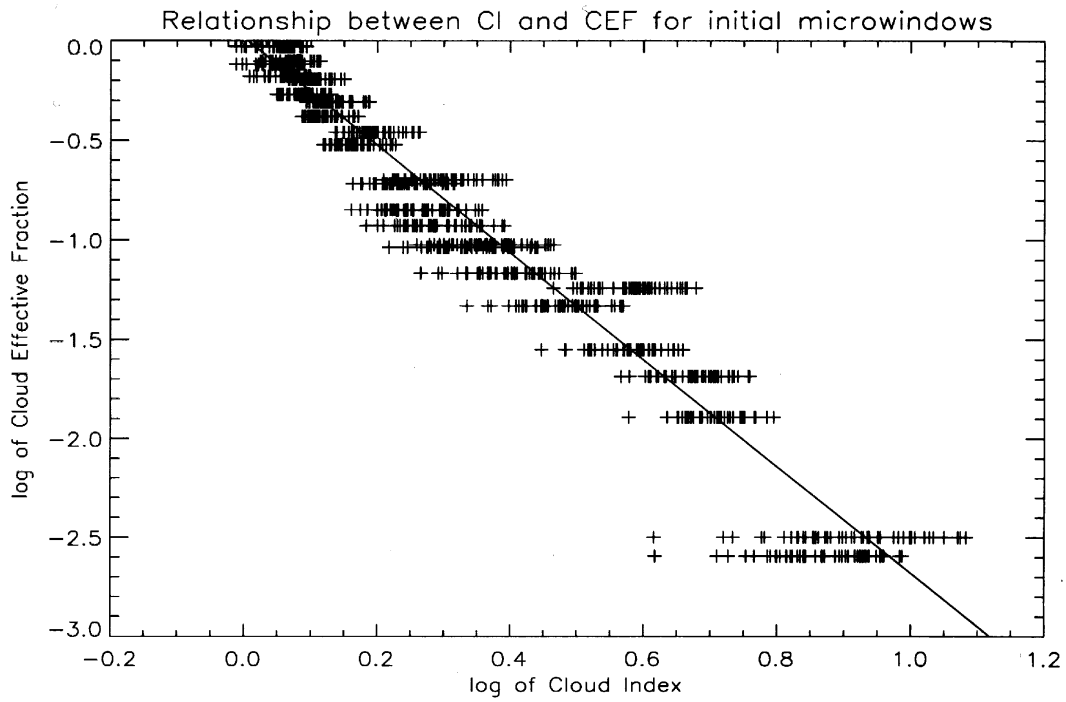

*Figure 5: Plot of log_{10}(CI) against log_{10}(CEF) using the MW pair 788 - 796 with 832 - 834. The best fit line is log_{10}(CEF) = 0.0149579 - 2.69564 * log_{10}(CI)*

A program was then developed to ascertain the values of the constants a and b, and to subsequently calculate the RMSE of the relationship. Before viewing the code, however, it is necessary to introduce a new concept which will play a key role in all RMSE calculations: instrument noise.

No instrument is perfect. That is to say, no instrument can measure its target flawlessly and with absolute precision, due to experimental uncertainty. The calculation of the magnitude of the noise comprises several discrete stages.

1. The RFM-simulated radiances include no noise contribution, so uncertainty must be added manually. In the case of the real MIPAS instrument, each radiance reading for each frequency is subject to an uncertainty modelled as 25 nW/cm^2 sr cm^{-1}. In reality, MIPAS' associated noise value ranges from around 50nW/cm^2 sr cm^{-1}, to 4.2nW/cm^2 sr cm^{-1} towards the shorter wavelength end of the spectrum, although testing has suggested that this may be an overestimate by as much as 100% [6]. It can be seen, therefore, that noise estimation is an imprecise art; the value of 25 nW/cm^2 sr cm^{-1} was selected as an average.

2. Each MIPAS radiance measurement gives us the 'true' value plus some random error. This error has a normal probability distribution, and hence the probability that it equals E is:

$$P(E)=\frac{e^{\frac{-E^2}{\sigma^2}}}{a}$$

Where σ^2 is the variance of the E value, and 'a' is a function designed to ensure that the total area under the probability density function is 1 (the probability of E having a value is one).

$$a=\int e^{-x/\sigma^2}\,dx$$

Where x is the 'true' radiance value.

Thus,

$$\int_{-\infty}^{\infty} P(E)dE = 1 \quad (1)$$

Also, the mean value of the error E is 0 (there is equal probability that the error will raise the observed radiance value as lower it). Since the mean (expectance) of any random continuous variable is the integral of X * P(X):

$$E(E) = \int_{-\infty}^{\infty} E * P(E)dE = 0 \quad (2)$$

Similarly,

$$Var(E) = \int_{-\infty}^{\infty} E^2 * P(E)dE - (E(E))^2 \quad (3)$$

Now we consider taking more than one measurement. Assume that the desired outcome y is some function, f, of N measurements. Hence:

$$y = f(X_{1,} X_{2,} \ldots, X_n)$$

Each X measurement has its own standard deviation representing the spread of its values (the errors), but we desire a way to describe the standard deviation of the outcome, y, about its true value.

$$\sigma^2{}_y = \int (y_{observed} - y_{true})^2 * P(y)\,dy$$

Where $y_{observed}$ - y_{true} is the error in y.

We can expand the error as:

$$\frac{\partial y}{\partial X_1} * E_1 + \frac{\partial y}{\partial X_2} * E_2 + \ldots + \frac{\partial y}{\partial X_n} * E_n = \sum_{i=1}^{N} f_i * E_i$$

Where $f_i = \delta y_i / \delta X_i$

Therefore,

$$Var(y) = \int \int \ldots \int (f_1 * E_1 + f_2 * E_2 + \ldots + f_N * E_N)^2 * P(E_1)dE_1 * P(E_2)dE_2 \ldots P(E_N)dE_N$$

Upon expansion of the squared term, there will be two types of term: $f_i{}^2\, E_i{}^2$ and $2 f_i\, f_j\, E_i\, E_j$. However, the latter terms will be zero from the requirement of equation 2. The equation will become:

$$Var(y) = \int \int \ldots \int (f_1{}^2 * E_1{}^2 + f_2{}^2 * E_2{}^2 + \ldots + f_N{}^2 * E_N{}^2) * P(E_1)dE_1 P(E_2)dE_2 \ldots P(E_N)dE_N$$

$$Var(y) = \sum \int f_i{}^2 * E_i{}^2 * P(E_i)dE_i * \int P(E_j)\,dE_j \ldots \quad (4)$$

Taking the f_i outside of the integral, the integral will become equation 3, which equals σ^2. Also, the

second integrated term in equation 4 is one (due to the requirement of equation 1). The definition of the variance can therefore be completed as follows:

$$Var(y)=\sum_{i=1}^{N} f_i^{\,2}*\sigma_i^{\,2} \quad (5)$$

[All equations in 2: personal communication Anu Dudhia]

3. Returning to the uncertainty of interest to this project, we first desire to calculate the error associated with the mean radiance value within a particular MW. Thus y in equation 5 is considered to be the average of N radiance values:

$$y=\frac{\sum X_i}{N}$$

Where X_i is a particular radiance value within a MW. Therefore,

$$f_i^{\,2}=\left(\frac{dy}{dx}\right)^2=\frac{1}{N^2}$$

and

$$Var(\overline{radiance})=\sum_{i=1}^{N}\frac{\sigma^2}{N^2}=\frac{1}{N^2}\sum\sigma^2=\frac{1}{N^2}*N\sigma^2=\frac{\sigma^2}{N}$$

Where σ is the noise associated with each particular radiance observation, which is 25nW/cm^2 sr cm^{-1}. Therefore,

$$S.D.=\sigma=\sqrt{(Var)}=\frac{25}{\sqrt{N}}$$

This means that the more points are taken into consideration (the greater N is), the lower the uncertainty in the mean radiance. This suggests that MWs spanning a larger wavenumber range should be more reliable. For the operational MWs (those in current usage), MW1 is 8 wavenumbers wide. 40 radiance measurements are taken in each wavenumber range due to MIPAS' spectral resolution of 0.025 cm^{-1}, meaning that that 8 * 40 + 1 = 321 radiance points are taken into consideration to calculate the mean radiance in MW1. Thus:

$$\sigma_{x_1}=\frac{25}{\sqrt{321}} \quad \text{and} \quad \sigma_{x_2}=\frac{25}{\sqrt{81}} \quad (6, 7)$$

Where x_1 equals the mean radiance in MW1, and x_2 the mean radiance in MW2.

4. The CI, however, is the ratio of these mean radiances:

$$CI=\frac{\overline{radiance_{MW1}}}{\overline{radiance_{MW2}}}$$

Referring again to equation 5, we now consider y to be the CI. Thus

$$y=\frac{x_1}{x_2}$$

Therefore,

$$f_1=\frac{\partial y}{\partial x_1}=\frac{1}{x_2}$$

and,

$$f_2=\frac{\partial y}{\partial x_2}=-\frac{x_1}{x_2^{\,2}}$$

Thus,

$$Var(CI)=\frac{(\frac{25}{\sqrt{321}})^{2}}{x_2^{\,2}}+\frac{(\frac{25}{\sqrt{81}})^{2}*x_1^{\,2}}{x_2^{\,4}}$$

Since σ_1 and σ_2 represent the uncertainty in the mean radiances in MW1 and 2 respectively (as calculated in equations 6 and 7).

5. The x-axis on figure 5, with which the best fit line and RMSE are calculated, is $\log_{10}$(CI). Again invoking equation 5, consider y to be $\log_{10}$(CI), and σ^2 to be Var(CI):

$$Var(\log_{10}(CI))=(\frac{\partial \log_{10}(CI)}{\partial CI})^{2}*Var(CI)=\frac{Var(CI)}{(\ln(10)*CI)^{2}}$$

Since:

$$Var(CI)=(\frac{x_1}{x_2})^{2}*(\frac{(\frac{25}{\sqrt{321}})^{2}}{x_1^{\,2}}+\frac{(\frac{25}{\sqrt{81}})^{2}}{x_2^{\,2}})$$

it follows that:

$$Var(\log_{10}(CI))=(\frac{1}{\ln(10)})^{2}*(\frac{(\frac{25}{\sqrt{321}})^{2}}{x_1^{\,2}}+\frac{(\frac{25}{\sqrt{81}})^{2}}{x_2^{\,2}})$$

6. The final aspect of the uncertainty for each x-coordinate is multiplication by the square of the gradient of the best fit line, to convert uncertainty in the x direction into uncertainty in the y (CEF) direction. Thus:

$$Var(\log_{10}(CEF)) = \left(\frac{1}{\ln(10)}\right)^2 * \left(\frac{\left(\frac{25}{\sqrt{321}}\right)^2}{x_1^2} + \frac{\left(\frac{25}{\sqrt{81}}\right)^2}{x_2^2}\right) * B^2$$

Where x_1 and x_2 are the mean radiances in MW1 and 2 respectively, and B is the gradient of the best fit line.

The uncertainty in the $\log_{10}$(CI) value, being dependant on the observed mean radiances, varies with the spectrum under scrutiny. Hence, for each point on the CI-CEF graph, the uncertainty will be added to the RMSE resulting from the imperfect nature of the best fit line. The contribution from the latter is the square of the vertical displacement of the actual CEF value for that spectrum type from the CEF value predicted (for the particular CI value) by the best fit line. The RMSE is the square root of the sum of these values. The line parameter and RMSE calculation program is reproduced in appendix 4.2.

IDL prints 0.181374. The reader is forgiven for harbouring uncertainty concerning the meaning of this result - it is dimensionless, and as yet has no similar results for comparison. A conceptual explanation would be that it is approximately 1% greater than the mean vertical distance between the data points and the line (the additional 1% originating from the noise). RMSEs calculated in the following section by a similar procedure, but for different MWs, will enable comparison.

5.2 Systematic CI and RMSE retrieval for potential A band MWs

It is now possible to initialise the attempt to improve on this value by considering different MW positions. It is not yet known what the approximate optimal width of the MWs are - a greater width will result in a lower noise contribution (more points are taken into account), but are also more likely to include gaseous emission and absorption lines, distorting the results by introducing a dependence on the concentration of these gases. Therefore, several MW widths were tested, starting with 1 wavenumber. For every possible combination of MWs of width 1 in the A band ($(970 - 685)^2 = 81225$ combinations in all), the CI was calculated for each of the 1296 simulated spectra. The code performing this is displayed in appendix 4.3. Appendix 4.4 contains the program that calculates the RMSE (of the same $\log_{10}$(CI)-$\log_{10}$(CEF) relationship as before) for each MW combination.

The lowest RMSE (representing the strongest correlation and hence most promising MWs) was found to be 0.160100 for the pair 774 - 775 and 819 - 820 cm^{-1}, a significant 11.7% improvement on the initial MW RMSE. This process was repeated for all potential MWs of width 2 and 3 wavenumbers respectively. The lowest RMSE for width 2 MWs was 0.170933 (for the MW pair 774 - 776 and 830 - 832), and for width 3 was 0.173282 (for 778 - 781 with 829 - 832). This technique was further applied on MWs of width 1 but with upper and lower bounds coinciding with half a wavenumber (as opposed to a whole wavenumber as above), achieving a minimum RMSE of 0.161079. The code for these variations is very similar to that for MWs of width one, so will not be included in the body of this narrative. The relationship between log10(CI) and log10(CEF) for the pair 774-775 and 819-820 (being the most favourable MWs located thus far) is shown is figure 6.

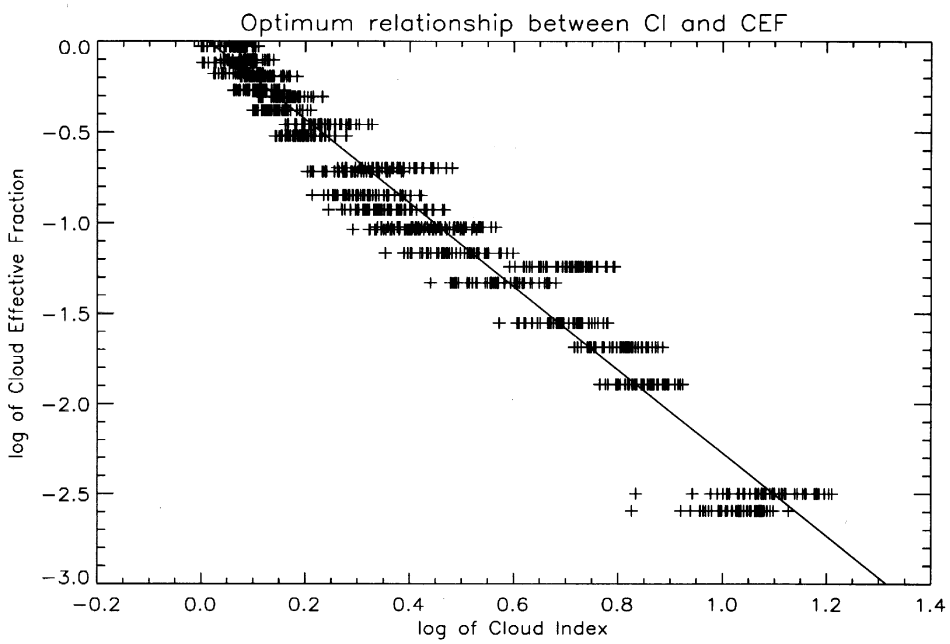

*Figure 6: Plot of log_{10}(CI) against log_{10}(CEF) using the MW pair 774 - 775 with 819 - 820. The best fit line is log_{10}(CEF) = 0.0301304 - 2.30472 * log_{10}(CI)*

Superficially, this appears very similar to figure 5, although it is possible to observe reduced vertical deviation of the points from the best fit line, particularly in the region of high CI. Note that all key results are reproduced in the table in the conclusion.

Although only the best pairs have been mentioned here, the top 37 results are published in appendix 1 for reference. There are several important points to note regarding these top MWs. Firstly, in appendix 1.1, the MW2 pair 819 - 820 features in 18 of the 37 pairs, including 90% of the top 10. The only other MW2 (cloud-dependant) positions appearing at all are 831 - 832 (occurring 12 times), 832 - 833 (occurring 6 times), and 830 - 831, appearing just once in 31st place. The position of the first (cloud-independent) MW, however, is much more variable - no favourite position is easily identifiable, and there are very few repeats, suggesting that the RMSE depends more on the position of MW2 than MW1. This is because the radiance value of MW1 does not depend on the nature or extent of cloud contamination, as illustrated by figures 1 and 2. The spectral region from 750 cm^{-1} onwards, on the other hand, varies considerably, and the magnitude of this change is dependant to a large extent on the exact positioning of MW2 within it. As an example, consider a simple comparison between the case of very thick cloud completely filling the FOV, and no cloud. In the latter case, the CEF will be zero, and we would hope that this would be reflected in a very high CI. This could be done either by having a large numerator (ie high radiance within MW1), or low denominator (radiance in MW2). However, in the thick cloud case, we wish the CI to be low. If we picked an MW1 region with high radiance to identify lack of cloud, we would now find that the CI was still high even in the thick cloud case as the radiance values do not change in this region of the spectrum. Thus it can be seen that CI-CEF correlation strength is not particularly dependant on MW1 position - a position useful for the detection of clear spectra is contrary to that required for the detection of cloudy spectra. However, this paradox can be avoided in MW2. For the identification of clear spectra, the radiance in MW2 should be as low as possible, whilst it should be as high as possible for the cloudy case. In the cloud-infected part of the cloudy spectrum, the radiance is greater at lower frequencies, so the optimal position of MW2 is in a region of low radiance without cloud, with bias also given to lower frequencies. It can be seen that 819 - 820 fits this perfectly - the region from approximately 819 - 825 has the lowest radiance in the entire clear spectrum, so the lower wavenumber part of this, 819 - 820, is selected. It is important to note that average radiances are used, and hence the radiance spikes (gaseous emission lines) are also taken into account. Although the regions 800 - 820 and 940 - 970

have approximately equivalent lowest radiances in the clear spectrum, their lines are much higher, so the mean radiance within MWs in those regions is also higher.

The seemingly second best MW2 region, 830 - 833, can be explained in a similar fashion. Careful observation of this region in figure 1 will reveal that it too has a very low mean radiance (the lowest radiance in this region is higher than 819 - 825, yet the emission lines are less pronounced). However, this is not quite as good as 819 - 825 because it has a lower radiance in the cloudy spectrum, so will not yield quite as low a CI in the cloudy case.

Appendix 1.2 shows that the same MW2 regions are favoured when the MW bounds rest on half a wavenumber. However, the slightly lower position of 817.5 - 818.5 is quite prevalent, appearing 10 times in the top 37. It is likely that this is placed in exactly the correct position to avoid including any emission lines in the clear spectra, thereby attaining a very low mean radiance in the clear spectra. The positions 817 - 818 and 818 - 819, although very nearby, include an emission line on the left and right, respectively, so do not feature in appendix 1.1.

It is immediately apparent from appendix 1.3, and especially 1.4, that, with wider MWs, the MW2 region around 830 is favoured more than that around 820, as was predominant before. 21 of the 37 are very close to 830 with MWs of width 2 (that is, lower bound on 829, 830, 831 or 832), whilst this figure rises to 29 for MWs of width 3 (including 8 of the top 10). Wider MW2s around 820 would necessarily include several reasonably high emission lines (extending to around 800 nW/cm^2 sr cm^{-1}), significantly raising their clear mean radiance and thus lowering the clear CI. However, in the region immediately around 830 cm^{-1}, the highest emission line reaches only around 400 nW/cm^2 sr cm^{-1}. This offsets having a slightly lower mean radiance in the cloudy case.

It is also noticeable that the exact positioning of MW2 is not quite as important with MWs of width 2. Whilst only 4 distinct pairs appear in the top 37 of appendix 1.1, 9 feature in appendix 1.3. These are all possible positions in the regions 820 - 826, and 831 - 835 (which, to reinforce earlier points, are all in regions of very low radiance when there is no cloud). Whilst width 1 MWs can be positioned exactly to avoid all emission lines (and only a select few which can do this feature in the top 37), width 2 MWs will always include a few such lines. 5 distinct MW2 positions appear in appendix 1.4, in the regions 822 - 827 and 832 - 837. Although these regions are almost identical to those from appendix 1.3, the larger width of the MWs means that fewer permutations can fit in. Connected to this, it was observed that there were, on average, taking into account the cases where the bounds were both on a whole wavenumber and half a wavenumber, 77 MW combinations of width 1 with RMSE lower than 0.2. However, there were 113 such combinations for MWs of width 2, and 119 for MWs of width 3. This further highlights the fact that MW2 positioning is more important for smaller MWs - after the few best ones had been considered, the quality rapidly decreased.

It is also useful to visualize the spectral regions giving the lowest RMSE, as the quoted MW positions above and in appendix 1 give an incomplete indication of RMSE distribution. Therefore, a series of 4 contour plots were synthesized showing the rough RMSE value generated by each of the spectral MW positions. One plot was made for each of the four MW sizes. Note that the white regions correspond to positions giving an RMSE greater than 0.5 (consideration of such excessively high RMSEs is unnecessary). A key linking the nature of the colouration to the RMSE range follows.

Colour	***RMSE***
Black	*0.15 - 0.20*
Purple	*0.20 - 0.25*
Blue	*0.25 - 0.30*
Dark Green	*0.30 - 0.35*
Light Green	*0.35 - 0.40*
Yellow	*0.40 - 0.45*
Red	*0.45 - 0.50*

NB *The distinction between the two shades of green is apparent only upon close inspection*

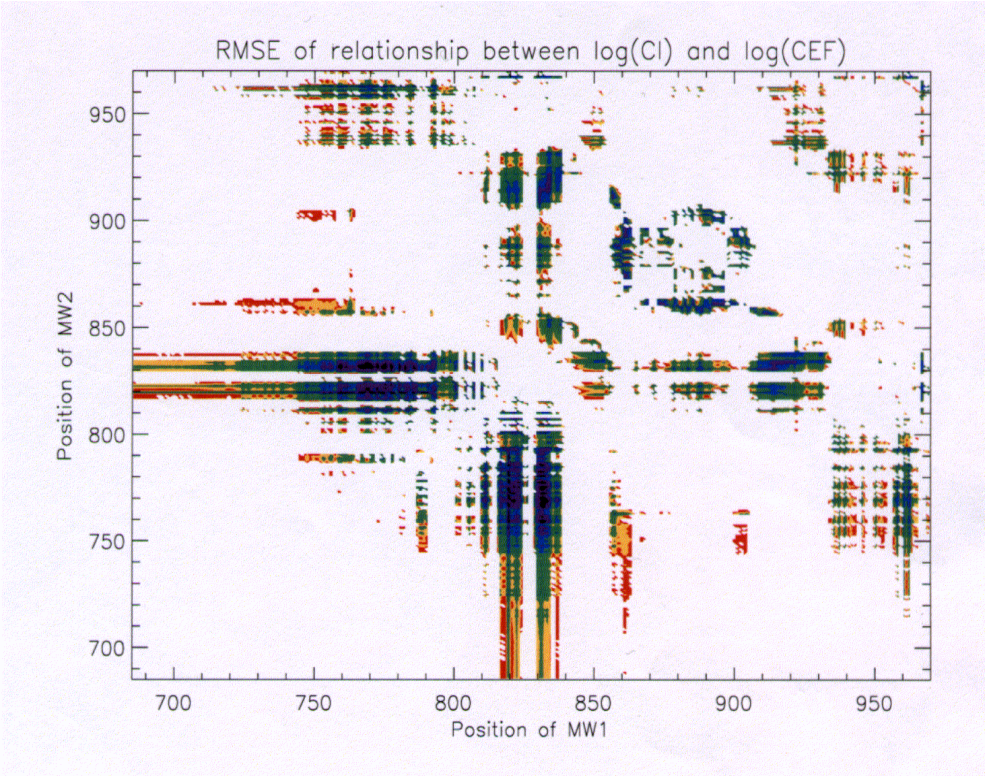

Figure 7: Contour plot indicating approximate RMSE values obtained by MWs of width 1 wavenumber located across the A band

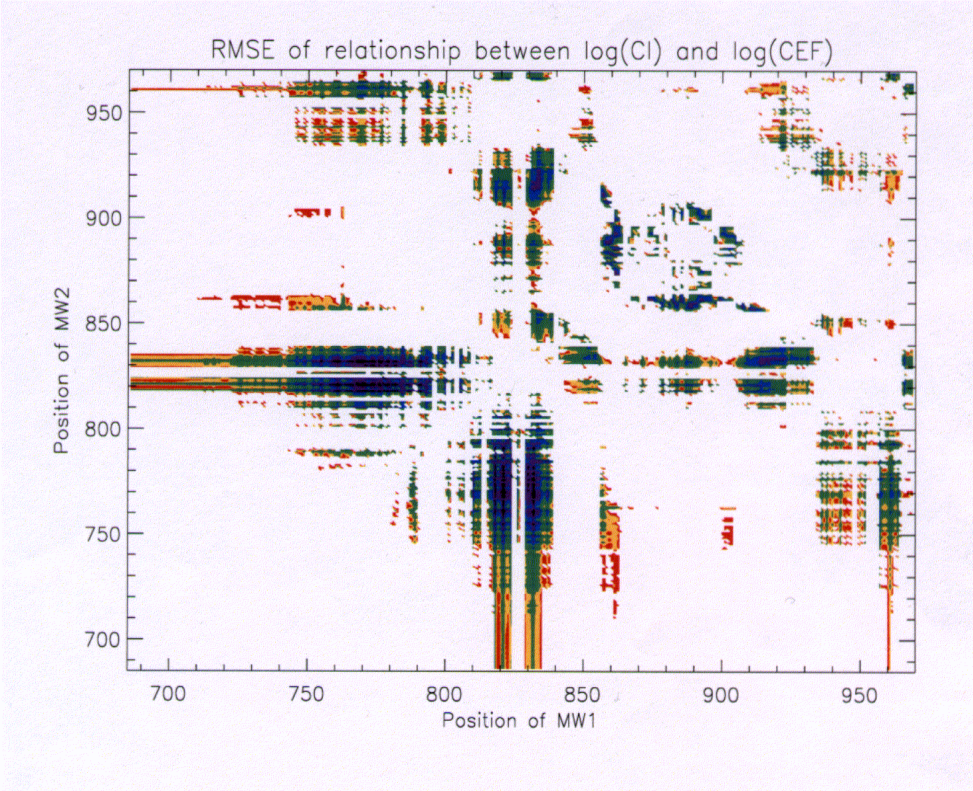

Figure 8: Same as above, but pertaining to MWs with bounds on half a wavenumber

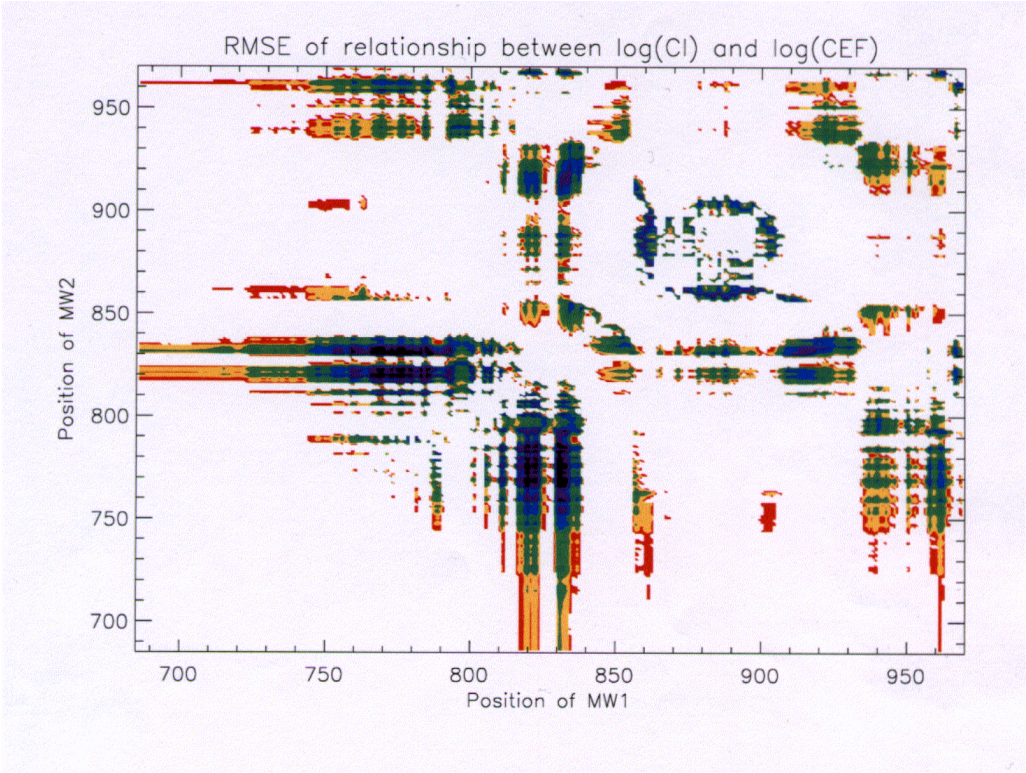

Figure 9: Width 2 wavenumber MWs

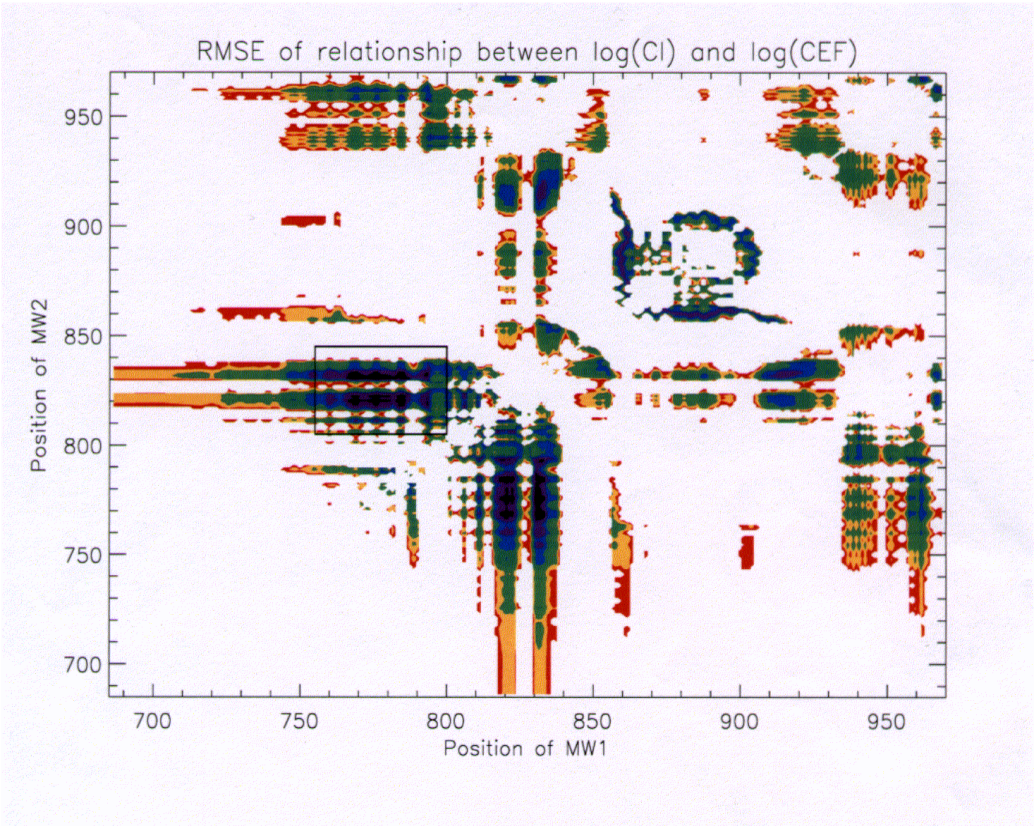

Figure 10: Width 3 wavenumber MWs

These results are encouraging not only in that they confirm the existence of 'better' MWs (at least for this particular purpose) than those suggested by Spang and Remedios, but also that they affirm the existence of a definitive region within the A band where consistently low RMSEs may be attained for any MW width. This permits us to focus our efforts within this region, which spans MW1 bounds between approximately 755 - 800 and MW2 bounds 805 - 845 (as delimited by the rectangle plotted over figure 10). Additional detail of this region is provided below by two plots showing this region (for width 1 and width 3 MWs, respectively) under greater magnification.

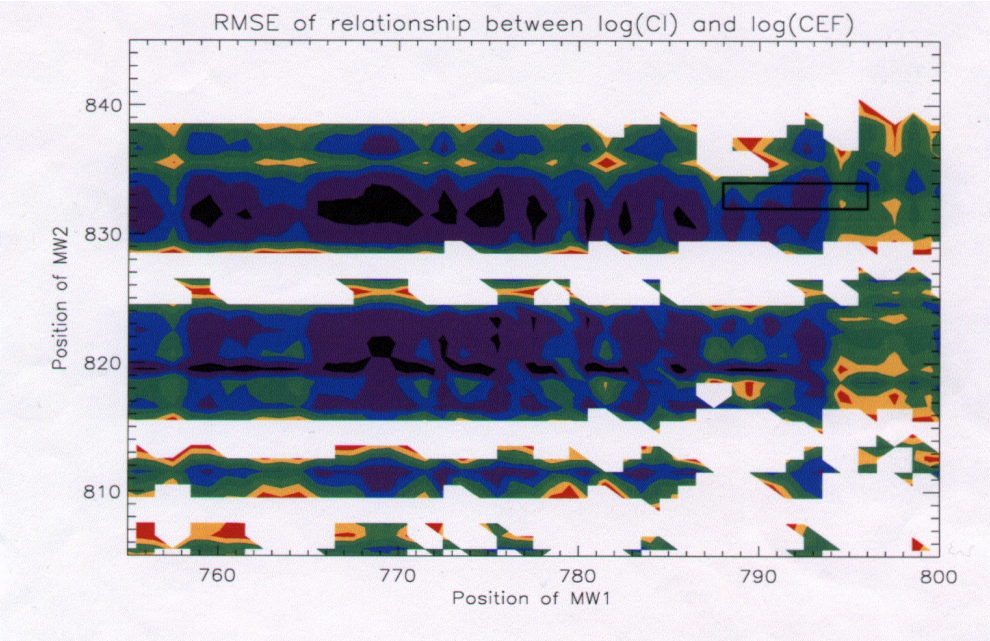

Figure 11: Detail from figure 7 of MW1 spectral region 755 - 800 cm^{-1}, and MW2 region 805 - 845 cm^{-1}. The rectangle indicates the position of the operational MWs (788 - 796 cm^{-1} with 832 - 834 cm^{-1}).

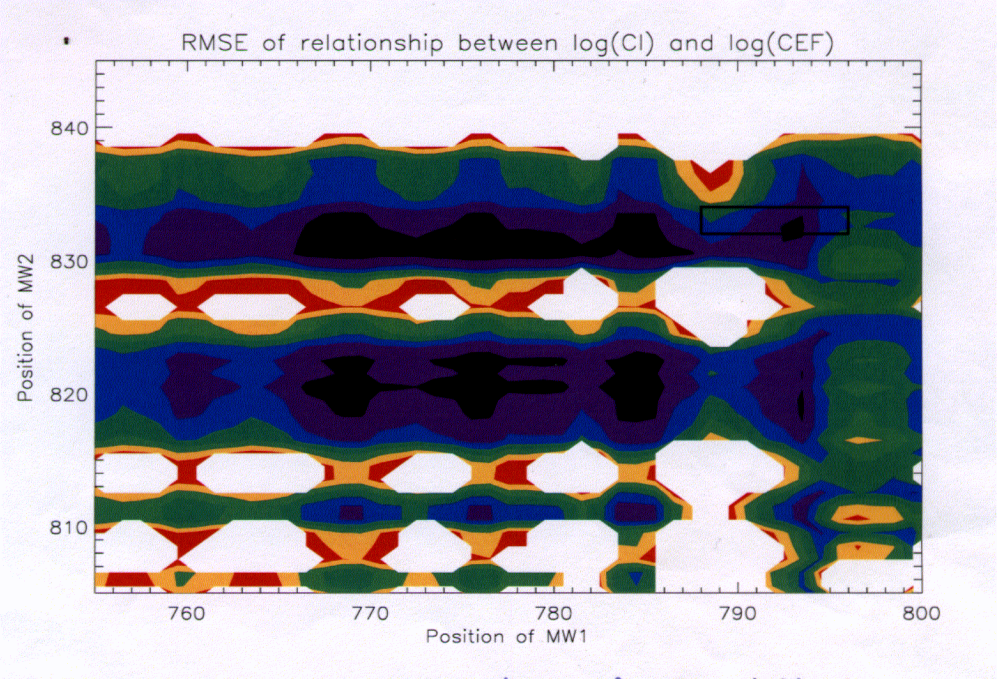

Figure 12: Detail from figure 10 of MW1 spectral region 755 - 800 cm^{-1}, and MW2 region 805 - 845 cm^{-1}

The first aspect to notice about these contour plots is that they are symmetrical about the line y = x. This is because the RMSE of the log(CI)-log(CEF) relationship is the same if log(CI) is calculated as log(MW1 / MW2) or log(MW2 / MW1). In the latter case, the correlation is positive, although the same deviations of the points from the best fit line are observed. In general, however, we designate MW1 to have a smaller wavenumber value than MW2, and thus consider the region above the line y = x. Notice also that no colour is observed along y = x. This represents MW1 coincident with MW2. The cloud index is thus always 1, and so no useful information can be obtained. The second point is that the bias towards MW2 positions of 820 or 830 is immediately obvious in all of the plots as a horizontal line of colour extending from these MW2 points. The optimum corresponding MW1 positions are between 760 and 790 cm^{-1}. Note also that the only other dominant horizontal lines on the plots occur around 940 and 960 cm^{-1} . Referring back to figure 1 it can be seen that this is also a region of low clear radiance (especially around 960 cm^{-1}, where, on the contour plots, streaks of blue may be observed). Finally, it can also be seen that the contour plots for MWs of width 3 and 2 are more colourful than the others. This shows that a wider range of regions give RMSEs below 0.5, and reinforces the fact that the precise positioning of larger MWs is less important than smaller ones.

5.3 Iterative techniques for further RMSE improvement

It is highly probable that the lowest RMSE obtained thus far, 0.160100, can still be lowered - after all, the program which calculated it considers MW position changes in coarse 40 spectral point (1 wavenumber) steps. An iterative method was adopted to attempt further improvement. Fundamentally, the RMSE corresponding to eight MW boundary changes (an increase in the upper bound of MW1 by one spectral point [0.025 cm^{-1}], a decrease in the same bound by 1 point, and similar changes for the lower bound of MW1, and both bounds of MW2) was measured. The change which gave the lowest RMSE (which the additional stipulation that it also reduced the RMSE below that obtained by the MW bounds without any change) was accepted, and the iteration repeated on these new MW boundaries. This continued until none of the 8 changes improved upon the existing RMSE. The code may be found in appendix 4.5.

The system settled on an RMSE of 0.1579820 (1.34 % improvement on 0.160100), terminating after 6 iterations on MWs: 774.075 - 775 (MW1) and 818.95 - 819.975 (MW2). The poor improvement was perhaps a reflection of the diminutive size of the boundary changes tested each iteration - only an area extremely localised around the defined boundaries could be explored, limiting the scope for significant improvement. With this in mind, the code was augmented by the construction of an external loop permitting the user to vary the magnitude of the changes. The changes would commence at 0.25 cm^{-1}, permit iteration to convergence, and then repeat with boundary changes of 0.15 cm^{-1}, and then again with 0.1 and 0.05, before terminating on 0.025 cm^{-1}, as before. This allowed a somewhat wider region to be tested, and afforded an improvement by revealing an RMSE of 0.15668215 at MWs of 774.075 - 775 and 819.175 - 819.95 (0.823% improvement on previous best). The code is published in appendix 4.6; it will be noted however that its general form is somewhat modified from that found in appendix 4.5, despite performing a very similar task in many respects. The latter is streamlined for the usage of 0.025 cm^{-1} boundary changes, and generalization to permit user-defined changes necessitated the observed alterations.

No further progress could be made with this code, despite extensive experimentation involving the relocation of the initial MW boundaries to be iterated upon into adjacent regions of low RMSE (as illustrated by figures 7 through 10), and modification of the magnitude of the boundary changes. The cause of this is perhaps the inherent disadvantage of iterative methods in general to descend into local minima with no consideration of the possibility of the existence of other, perhaps better, minima nearby. To address this limitation, the technique of simulated annealing was explored.

5.4 Simulated Annealing

Simulated annealing builds on the iterative techniques developed above, with one major difference: there is a probability of accepting new MW boundaries even if this raises the RMSE.

The statistical technique of simulated annealing draws its inspiration from thermodynamics, and in particular crystal growth in metals. Metals comprise numerous distinct crystals, called grains. The metal ions within a grain are aligned with each other, although they adopt arbitrary orientation relative to the ions in adjacent grains. Grains form when the metals solidify from a molten state, and the size of the grains produced is highly dependant on the rate of cooling. In metallurgy, annealing describes the technique of large grain generation by heating followed by slow cooling. Ions become freed from their initial position, which is a local minimum of internal energy, and wander through states of higher energy. As the temperature falls, they begin more and more to head in a 'downhill' direction regarding energy, before, ideally, settling in one of the deepest energy minima. This creates a thoroughly ordered metal artefact with few defects. (This is contrasted with the technique of quenching, in which small grains are created by the rapid immersion of the metal into cold water). Simulated annealing mimics this process: in this case, the initial MW boundaries are replaced by random, yet nearby, ones, and the probability of accepting these new boundaries is defined as follows:

$$P(accept) = e^{-\frac{(FinalRMSE - InitialRMSE)}{(T * const)}}$$

where T is an defined parameter analogous to temperature, and const a real constant. The RMSE is the analogue of energy. The probability of acceptance is higher if the discrepancy between the initial and newly presented RMSE is smaller. It is, however defined as 1 if the final RMSE is less than the initial RMSE. The temperature is multiplied by a factor less than 1 after a certain number of iterations, and thus the probability of accepting less favourable MW boundaries falls as the program progresses. There are a number of ways in which the boundaries could be changed randomly; two were tested. The first, which has the greater similarity with the previous iterative methods, retains the idea of 8 consecutive changes, but makes the step size random yet directly dependant on temperature. Thus the system will initially adopt large MW boundary changes (allowing it to explore large areas), which gradually become smaller as T decreases (so that, towards the end when it is hoped that the optimal region has been selected, only very fine modifications are made). An 'if' loop ensures that the size of the boundary changes never falls below 1. See appendix 4.7 for the code pertaining to this version. The second version (appendix 4.8) changes instead both the middle value of the two MWs, and their width (again, randomly yet dependant on temperature).

It can be seen that there are numerous parameters (initial T, 'const', T multiplication factor, the number of iterations between T diminutions, and the multiplication factor for the step sizes), all of which must be defined by hand before commencing the running of the program. In short, no rationale was developed during the course of this project for their values. It was impossible without a lengthy trial and error process to optimise the selection of their values, and with it the annealing process; this represented a major problem for both programs. So much so that, despite considerable testing of various permutations of these parameters (which are documented, along with their result, in appendix 3), the outputted RMSE was almost invariably higher than that for the defined RMSE boundaries. Specifically, the main problem regarding the first version was that the boundaries never changed by a great amount in the long term - for example, the upper boundary of MW1 is increased in the first of the 8 changes, and decreased in the second. Despite the randomization, the net change is often insignificant. This resulted in the result being highly dependant on the initial boundaries; ideally, the system should tend towards the same optimum positions regardless of starting point. This was not so much of a problem for the second program (although the random nature could still permit zero change after two iterations), but this was crippled by a further limitation. Namely, almost every boundary change was accepted. Towards the beginning, this is to be expected, even desired, but towards the end, as the temperature decreases, the system should begin to accept only RMSE improvements.

However, as the temperature fell, so did the size of the MW changes. Hence the magnitude of the RMSE change decreased too, raising the probability of accepting the new RMSE, even if it was higher than the previous one. In practice, these contrasting factors (reduced T and reduced value of 'Final RMSE - Initial RMSE') seemed to cancel each other out, and so the probability of accepting worse MW boundaries remained very high.

Specific recommended improvements regarding the simulated annealing technique are detailed towards the end of this paper, but suffice it to say here that no improvement on 0.15668215 was obtained.

This concludes the attempt to optimise MW positioning for the maximisation of the strength of the CI-CEF correlation, with the best MWs remaining at 774.075 - 775 and 819.175 - 819.95 (RMSE = 0.15668215). From now on, MW worth will have a different measure.

6. MW optimisation through CI thresholding

6.1 Percentage of clear spectra lost given threshold at maximum CI of cloudy spectra

It was described in earlier sections that a CI threshold is set to distinguish clear spectra from cloudy spectra. A spectrum with a CI less than or equal to the threshold would be discarded. The issue of the selection of the threshold was kept rather vague - in practice one would tend to set the threshold with priority given to ensuring that all cloudy spectra had been eliminated, rather than attempting to retain as many clear spectra as possible. For many purposes it would therefore be suitable to define the threshold as the highest CI value of any cloudy spectrum (thus all cloudy spectra would be identified and could be discarded); in this case a suitable measure of MW value would be the fraction of clear spectra which have a CI below this value, and would therefore be lost. Better MWs would give a lower fraction. This fraction was calculated for each of the 81225 possible permutations of 1 wavenumber wide MW positions (width 1 MWs were selected as a starting point as they afforded the lowest RMSE, in section 5). By this reckoning, the optimum MW pair is 946 - 947 with 943 - 944, losing 22.9% of the clear spectra. It will be observed, however, that this pair is in a completely different region of the A band from those selected on the basis of low RMSE (and indeed figure 7 shows that it is in fact in a region of very poor RMSE), yet one would expect that MWs exhibiting low RMSE would also afford clear distinction between clear and cloudy spectra. The relationship between log(CI) and log(CEF) for this MW (with points representing, as before, the 1296 simulated spectra) is illustrated in figure 13. It can be seen that approximately one quarter of the clear spectra (those with a CEF of -2.5) have a CI value lower than the threshold set at the greatest CI obtained from any cloudy spectrum. The red line on figure 13 indicates the position of this threshold.

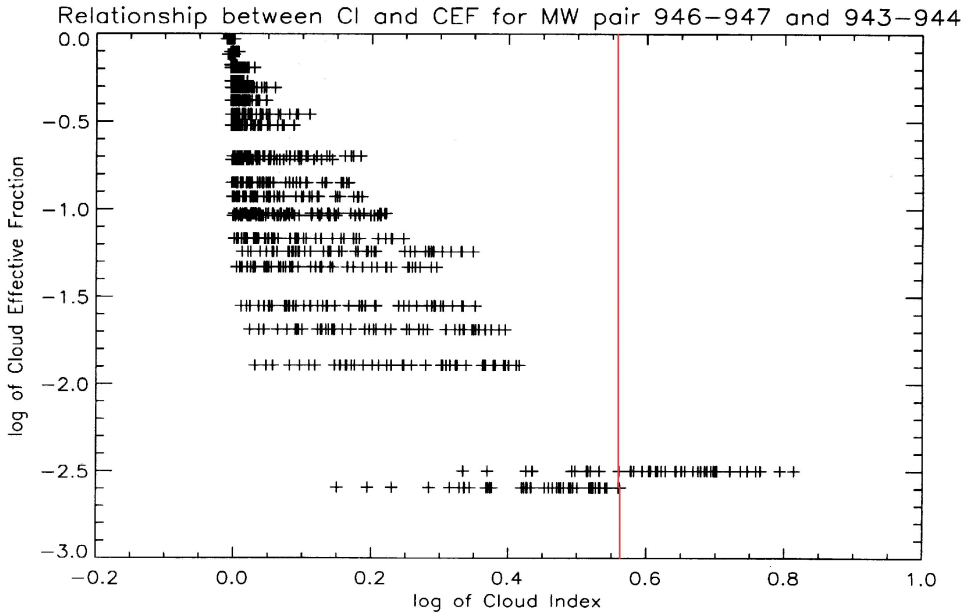

Figure 13: Plot of log_{10}(CI) against log_{10}(CEF) using MW pair 946 - 947 with 943 - 944

If one accepts the discord of this result and those obtained in section 5.2 as a valid concern, then analysis of the source of the large discrepancy in MW positions is imperative. Referring back to figure 6, it is evident that, although the MW pair 774 - 775 with 819 - 820 does give a poor result based on the above criteria, it would receive a much more favourable assessment if the CI threshold excluded the lowest rung of cloudy spectra (those with log(CEF) approximating to -2.6). These correspond to cloudy spectra with a cloud top height of -1.5 (i.e. only the bottom 8th of the MIPAS FOV is cloud-filled) and extinction coefficient of 0.001 (i.e. near-negligible radiative effect). It is quite likely that during actual MIPAS operation, such spectra would not in fact be discarded as being too cloudy, as such cloud would create minimal distortion of MIPAS retrievals. It may therefore be reasonable to redefine the threshold as the highest CI of any cloudy spectrum bar those with the above characteristics. With this modification effected the test was repeated: the results were indeed considerably different. Now, tied in first place with only 0.694% of clear spectra lost, are the MW pairs 773 - 774 with 819 - 820, 788-789 with 819 - 820, and 807 - 808 with 831 - 832 cm^{-1}. It is encouraging to note that these three positions are, in addition, in regions of relatively low RMSE. (Indeed, only 2.08 % of clear spectra are lost by the 1 wavenumber wide MW pair giving the lowest RMSE [774 - 775 with 819 - 820]). It was therefore concluded that the very thin cloud cases should not be included in investigations of this nature, and from here on, the term 'cloudy' will not encompass these cases.

The effect of noise on these findings was then considered. There is no rule regarding how best to effectuate this - a first approximation of its effect was as follows: the nominal CI noise value (that is, following numbers 1 through 3 from section 5.1) for each spectrum was calculated. The noise values for the clear spectra were then subtracted from their CIs, whilst the noise for the cloudy spectra was added to their CIs, thus bringing the clear and cloudy CI values closer together by a noise-dependant amount. The fraction of clear spectra lost was subsequently re-evaluated. The code which performed these calculations is published in appendix 4.8.

The only one of the previous three best MWs pairs to have avoided losing additional clear spectra is the pair 788 - 789 with 819 - 820: 773 - 774 with 819 - 820 lost an extra 1.39 % of clear spectra, 807 - 808 with 831 - 832 an extra 3.47 %. Although this test was not explicitly performed on the initial MW pair, it is evident from figure 4 that this pair would receive an unfavourable assessment, perhaps losing as many as 20 %. Appendix 2.1 lists the 37 top results. It can be seen that,

as before, 819 - 820 is the most common MW2 position (appearing 12 times in the top 37), and the general positioning of the microwindows is similar to appendix 1.1. In particular, the favouritism shown to the regions around 820 and 830 is still apparent, for the same reasons as before. However, the position of MW1 fluctuates much more dramatically, with 9 of the top 37 existing beyond 800 cm^{-1}, 4 of which are also greater than 900 cm^{-1}. This can be explained by reference to figures 1 and 2. Firstly, a more favourable assessment will be given to MWs giving a lower cloudy CI threshold, which is achieved by having a lower mean radiance in MW1 for cloudy spectra. It can be seen from figure 2 that this occurs when MW1 has a higher spectral position (900 - 950 cm^{-1} seems particularly good). For clear spectra, we desire the CIs to be greater (so that they are not confused with cloudy CIs). An MW1 position in the region 685 - 750 cm^{-1} would be good for this purpose, although this would also produce a high threshold. In practice, some MW1 positions are found in each of these areas in the top 37. Notice, however, that the selected MW1 positions greater than 900 cm^{-1} also correspond to regions of high radiance in the clear spectrum (notably 918 - 919 and 920 - 921 cm^{-1}).

6.2 Inclusion of clear spectral CI mean and SD

Although useful as preliminary work, the above method has two major drawbacks, limiting the utility of the conclusions. Firstly, the CIs of all clear spectra are either classed as less than the threshold or greater than it, with no regard paid to their actual distance from it. Secondly, only the cloudy spectrum with the greatest CI is taken into consideration in the threshold calculation, whilst all other cloudy spectra are neglected. The first of these problems was addressed by the calculation of the mean and standard deviation of the clear spectral CIs. The formulation of the standard deviation term also included the noise contribution for each data point (see the code in appendix 4.10 for exactly how this was done). The number of standard deviations (SDs) between this mean and the previously ascertained threshold was calculated for each of the MW combinations. A higher result would indicate greater separation of the clear and cloudy spectra (thus, in practice, one would be less likely to confuse the two classes), and hence a better MW combination.

$$Result = \frac{\overline{CI_{clear}} - Threshold_{cloudy}}{\sigma_{clear}}$$

The result was encouraging in that it conformed closely to the results of previous methods - the greatest number of SDs (1.97184) was observed for the pair 773 - 774 with 819 - 820. Appendix 2.2 stores the top 37 results - the general pattern of placement of both MW1 and MW2 is very similar to that observed in appendix 2.1.

Interestingly, 95.0% of the MW combinations yielded a negative result, showing that, for these combinations, the mean of the clear CIs is less than the maximum CI of the cloudy spectra, and hence typical clear spectra would be lost. This highlights the necessity of careful MW selection methods based on a wide range of data, as the vast majority of MW positions are useless. To promote comparison between the MWs investigated in this project and those in current usage (788 - 796 with 832 - 834), this test was repeated on the latter through slight modification of the code (insufficient for its exhibition to be deemed necessary). A result of 1.1673792 is obtained, confirming that improved MWs have been located in this regard also.

6.3 Additional inclusion of cloudy spectral CI mean and SD

The methodology was further refined through the overcoming of the second aforementioned limitation. This was done by discarding altogether the explicit concept of a CI threshold; rather the mean and SD (including noise) of the cloudy spectra was also calculated, with the difference between the clear and cloudy means divided by the sum of the clear and cloudy SDs being the measure of separation. This was executed by a modified code, situated in appendix 4.11.

$$Result = \frac{\overline{CI_{clear}} - \overline{CI_{cloudy}}}{\sigma_{clear} + \sigma_{cloudy}}$$

The greatest result for any of the 81225 MW combinations was 1.58446 (corresponding to the pair 756 - 757 with 819 - 820). Appendix 2.3, listing the 37 best MW pairs by this assessment, reveals that the very high MW1 positions found in appendix 2.1 and 2.2 have disappeared, and the general positioning is now very similar to that found in appendix 1.1. This is because less priority is given to reducing the CI values of the thickest cloud cases, reducing the bias towards very low radiances for MW1 in the cloudy spectra.

The result for the initial MWs, however, is a considerably better 2.0336517, which is unexpected in light of the fact that the initial MWs have, in previous tests, consistently performed worse than those selected in this investigation. To elucidate this revelation, the constituent components of the two results were analysed in greater detail. A plot of log(CI) against log(CEF) for each MW pair highlights the major differences.

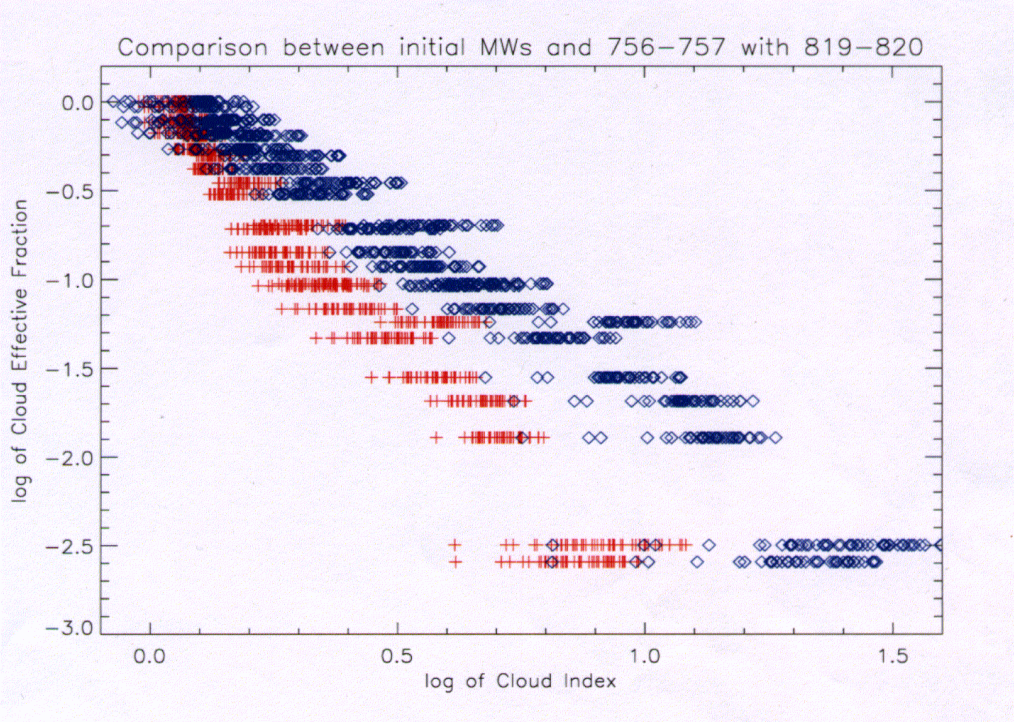

Figure 14: Plot of log_{10}(CI) against log_{10}(CEF) using operational MWs (red), and MW pair 756 - 757 with 819 - 820 (blue)

The most readily distinguishable difference is the greater steepness of the regression for the initial MWs. Therefore, although there was a much smaller difference between the clear and cloudy means for the initial MWs (6.3785 as opposed to 21.112), the sum of the SDs was also much smaller (3.137 compared with 13.325). Compounding this is the fact that, as the initial MWs are considerably larger than 1 wavenumber, they do not suffer as much from noise (with the effect of further reducing both the clear and cloudy SDs).

It may be wondered at this juncture whether the division of the mean difference by the SD sum is necessary, or indeed desirable. In our current design, we wish to maximise CI spread, yet a lower CI SD (producing a greater and hence more favourable result) is indicative of lower spread. It was therefore decided to experiment with the removal of the SD-comprised denominator, and subsequently reassess the best MW pair (this was achieved by simply removing all SD references in the above program). The greatest result is an exceedingly high 944.311 for the MW pair 685 - 686

with 943 - 944. The CI-CEF relationship is shown below.

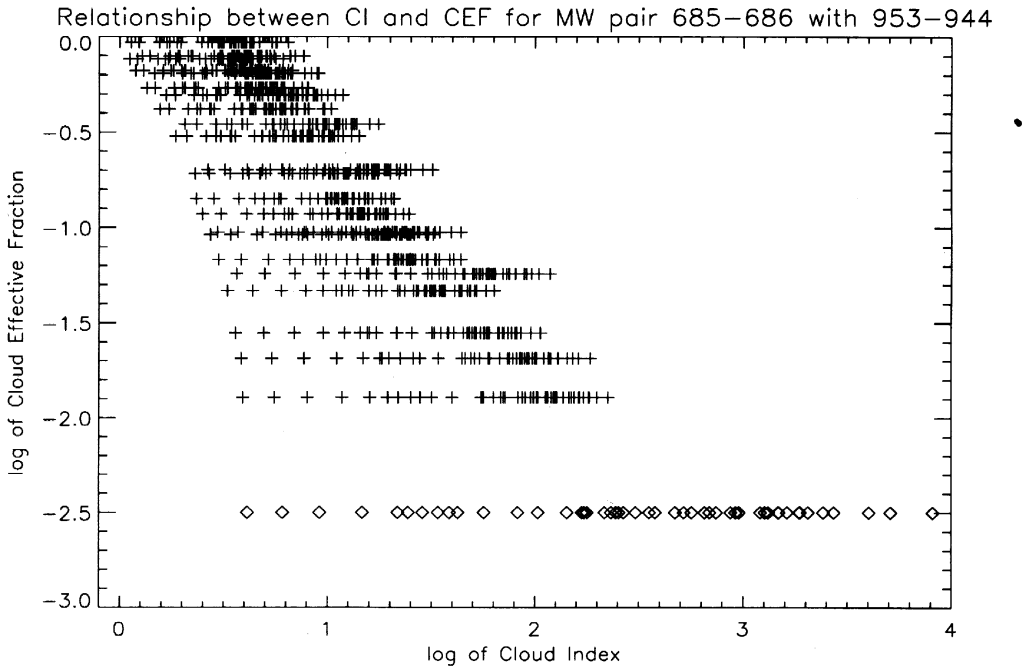

Figure 15: Plot of log_{10}(CI) against log_{10}(CEF) using MW pair 685 - 686 with 953 - 954. Clear spectral CIs denoted by diamonds, cloudy CIs by crosses.

The most striking feature of this relationship is the extreme spread exhibited by the clear spectral CIs (ranging from around 4.0 to 7900!); it is evident that any threshold set with the priority of discarding the vast majority of cloudy spectra would also cause the loss of innumerable clear spectra. It can be seen, therefore, that greater CI spread is not the sole objective - this is supplied in the above plot by several extremely high CI values, whilst there are also numerous low ones (as low as those obtained by moderately cloud-contaminated spectra). The SD ratio is necessary as it forces selected MW combinations to conform to more linear relationships by reducing the impetus for exaggerated CI spread. At the end of the day, it does not matter whether a spectrum has a CI of one greater than the threshold or several thousand greater, as it will be accepted either way. The ratio will therefore cause combinations receiving a favourable assessment by this test to also generate a low RMSE.

7. Summary and Conclusion

The key results are summarised in the following table.

	Result	**Result for operational MWs**	**Result for (next) best MW pair**	**Position of (next) best MW pair / cm^{-1}**	**% improvement**
Section 5 Lower better	RMSE	0.181374	0.156682	774.075 - 775 819.175 - 819.95	13.614
Section 6.1 Lower better	100 * (No. clear CI < max cloudy CI) / No. clear CI	≈ 20	0.694444	788 - 789 819 - 820	≈ 96.528
Section 6.2 Higher better	(Clear mean CI - max cloudy CI) / clear SD	1.16738	1.97184	773 - 774 819 - 820	68.912
Section 6.3 Higher better	(Clear mean CI - Cloudy mean CI) / (clear SD + cloudy SD)	2.03365	1.58446	756 - 757 819 - 820	OPERATIONAL MWs are 28.350 % better

The techniques in section 5 are intended for the determination of the exact optical properties of cloud filling a particular MIPAS FOV; their use therefore extends beyond merely disregarding cloud-filled spectra (which is the objective of section 6). The methods would, through the calculation of the CEF, aid in the documentation of the occurrence of different cloud types, and permit quantification of the radiative alterations effected by such cloud. It has been demonstrated that considerable improvement can be made on MW selection in this regard (13.6% improvement achieved). Pending continued experimentation with simulated annealing and other such statistical techniques, this project would recommend the adoption of the MW pair 774.075 - 775 and 819.175 - 819.95 when quantifiable information concerning the nature of the cloud in the FOV is required.

Whilst the methodology in section 5 represented a fairly self-consistent and integrated set of techniques, section 6 presented several methods for measuring essentially the same parameter, the clear-cloudy CI separation. It is therefore helpful to evaluate the reliability of each method relative to the others to ascertain which result is most trustworthy. The primary issue for consideration is the positioning of the CI threshold - sections 6.1 and 6.2 both consider this fixed at the highest CI value of any cloudy spectrum. In reality, however, this would not be the case. Rigid definition of the threshold at this point would indeed discard all cloudy spectra, but would also remove the maximum number of clear spectra. Efficiency is significantly improved if each case is considered on the basis of its own merits, allowing slight modification of the threshold to retain maximum identification of cloudy spectra whilst minimizing the number of clear spectra lost. Ultimately, the aim would be a compromise threshold based on data from numerous spectra, both RFM-simulated and MIPAS-collected. It is therefore believed that the methodology described in 6.3 (including the SD ratio) is the most reliable, as it takes all spectra into account and provides the most general information regarding their separation. This is intended to provide a basis for more detailed and spectrum-specific studies for the determination of the optimum threshold position in the future. In addition, the disappearance of the spurious high frequency MW positions suggests that MWs selected by this method will also exhibit low RMSE when tested by the methods of section 5. It must, then, be concluded that the initial MW pair (788 - 796 cm^{-1} and 832 - 834 cm^{-1}) is most suited to this task, and will therefore continue to remain useful when the sole aim of their usage is the distinction of these two spectral types. In the final analysis, they present a 28.3% improvement on the optimum 1 wavenumber wide MW pair discovered in this paper.

8. Suggestions for further work

1. The adoption of a linear $\log_{10}$-$\log_{10}$ relationship between CI and CEF was without experimental justification. Other function types (perhaps with an emphasis on polynomials, as suggested by [10]) should be tested with the aim of RMSE reduction.

2. The potential of the method of simulated annealing was never realized. Progress is likely to originate either from study of the effects of the numerous parameters involved, leading to their subsequent optimisation, or the adoption of an extensive trial and improvement scheme. In particular, it may prove fruitful to eliminate the dependence of the step sizes on T - they could either remain constant, or decrease with lower frequency that T does.

3. Section 6 considered MWs of width 1 only. After settling on optimum methodology for this objective, it would be useful to extend the analysis to other widths, and ultimately adopt an iterative procedure similar to those detailed in section 5 to further refine the MW boundaries.

4. Only two measures of MW value were explored in this investigation, each useful for a different objective. It would be useful not only to integrate the results from these two methods (thus developing a more comprehensive method of MW selection), but also to research other possible ways in which MWs could be assessed.

5. The RFM is only equipped to model cloud with a horizontal top. Although the majority of cloud types do exhibit such structure, we saw in section 3 that many (notably cumulus) do not. The augmentation of RFM procedures to include irregularly shaped cloud would be productive.

Appendix 1.1: Optimum MWs of width 1 cm^{-1} for RMSE minimisation

RMSE	MW1 Position	MW2 Position
0.16010	774–775	819–820
0.16172	785–786	819–820
0.16589	778–779	819–820
0.16674	770–771	819–820
0.16823	767–678	819–820
0.16931	771–772	819–820
0.16993	777–778	819–820
0.17008	777–778	831–832
0.17485	761–762	819–820
0.17505	781–782	819–820
0.17624	775–776	831–832
0.17650	759–760	819–820
0.17689	767–768	831–832
0.17691	770–771	831–832
0.17742	773–774	819–820
0.18013	774–775	831–832
0.18103	759–760	831–832
0.18122	766–767	819–820
0.18161	780–781	831–832
0.18251	775–776	832–833
0.18339	780–781	819–820
0.18437	785–786	831–832
0.18455	766–767	831–832
0.18529	763–764	819–820
0.18557	782–783	819–820
0.18596	769–770	831–832
0.18621	789–790	819–820
0.18639	777–778	832–833
0.18676	768–769	832–833
0.18772	772–773	832–833
0.18848	782–783	830–831
0.18849	760–761	819–820
0.18897	780–781	832–833
0.18934	772–773	821–822
0.18936	769–770	832–833
0.18961	768–769	831–832
0.18979	758–759	819–820

Appendix 1.2: Optimum MWs of width 1 with bounds coincident upon half a wavenumber

RMSE	MW1 Position	MW2 Position
0.16108	790.5-791.5	831.5-832.5
0.16393	775.5-776.5	831.5-832.5
0.16573	770.5-771.5	820.5-821.5
0.16594	778.5-779.5	831.5-832.5
0.16683	773.5-774.5	831.5-832.5
0.16901	767.5-768.5	831.5-832.5
0.17006	768.5-769.5	831.5-832.5
0.17013	771.5-772.5	820.5-821.5
0.17052	770.5-771.5	831.5-832.5
0.17147	770.5-771.5	817.5-818.5
0.17149	773.5-774.5	820.5-821.5
0.17206	760.5-761.5	831.5-832.5
0.17312	775.5-776.5	820.5-821.5
0.17366	778.5-779.5	820.5-821.5
0.17381	773.5-774.5	817.5-818.5
0.17421	780.5-781.5	820.5-821.5
0.17421	765.5-766.5	820.5-821.5
0.17476	760.5-761.5	820.5-821.5
0.17509	763.5-764.5	820.5-821.5
0.17519	775.5-776.5	817.5-818.5
0.17536	772.5-773.5	831.5-832.5
0.17561	781.5-782.5	831.5-832.5
0.17604	769.5-770.5	831.5-832.5
0.17627	778.5-779.5	817.5-818.5
0.17631	790.5-791.5	820.5-821.5
0.17690	781.5-782.5	817.5-818.5
0.17706	760.5-761.5	817.5-818.5
0.17744	772.5-773.5	820.5-821.5
0.17796	765.5-766.5	831.5-832.5
0.17799	771.5-772.5	817.5-818.5
0.17806	764.5-765.5	820.5-821.5
0.17868	781.5-782.5	820.5-821.5
0.17907	790.5-791.5	817.5-818.5
0.17918	772.5-773.5	817.5-818.5
0.17966	754.5-755.5	831.5-832.5
0.18034	780.5-781.5	817.5-818.5
0.18041	777.5-778.5	823.5-824.5

Appendix 1.3: Optimum MWs of width 2 for RMSE minimisation

RMSE	MW1 Position	MW2 Position
0.17093	774–776	819–821
0.17275	767–768	830–832
0.17462	778–780	831–833
0.17515	772–774	832–834
0.17549	772–774	830–832
0.17611	776–778	818–820
0.17634	785–787	819–821
0.17668	774–776	829–831
0.17711	769–771	830–832
0.17745	782–784	831–833
0.17956	769–771	832–834
0.17970	767–769	819–821
0.17994	768–770	830–832
0.18025	767–769	831–833
0.18037	765–767	832–834
0.18092	768–770	818–820
0.18125	767–769	819–821
0.18189	778–780	821–823
0.18209	771–773	822–824
0.18210	765–767	829–831
0.18211	773–775	830–832
0.18214	785–787	831–833
0.18293	785–787	832–834
0.18398	772–774	818–820
0.18406	776–778	819–821
0.18406	778–780	820–822
0.18421	774–776	821–823
0.18423	766–768	830–832
0.18423	782–784	831–833
0.18424	768–770	832–834
0.18446	769–771	818–820
0.18472	776–778	819–821
0.18507	774–776	821–823
0.18528	784–786	822–824
0.18533	782–784	829–831
0.18537	784–786	830–832
0.18682	774–776	831–833

Appendix 1.4: Optimum MWs of width 3 for RMSE minimisation

RMSE	MW1 Position	MW2 Position
0.17328	778–781	829–832
0.17455	773–776	829–832
0.17476	777–780	829–832
0.17561	772–775	829–832
0.17614	776–779	829–832
0.17651	781–784	829–832
0.17674	774–778	830–833
0.17735	779–782	829–832
0.17783	774–778	829–832
0.17837	767–770	830–833
0.17850	775–778	830–833
0.17944	768–771	830–833
0.18042	775–778	829–832
0.18065	774–777	819–822
0.18122	768–771	829–832
0.18142	784–787	830–833
0.18150	767–769	829–832
0.18168	768–771	819–822
0.18195	767–770	831–834
0.18213	766–769	830–833
0.18239	767–770	819–822
0.18287	766–769	829–832
0.18293	773–776	830–833
0.18364	775–778	819–822
0.18368	774–776	821–824
0.18375	783–786	830–833
0.18411	768–771	831–834
0.18430	773–776	819–822
0.18454	770–773	829–832
0.18495	771–774	829–832
0.18498	785–788	829–832
0.18515	765–768	829–832
0.18518	775–778	821–824
0.18529	769–772	829–832
0.18607	774–777	831–833
0.18636	780–783	829–832
0.18650	772–775	819–832

Appendix 2.1: Optimum MWs for maximum retention of clear spectra

% of Clear Spectra Lost	MW1 Position	MW2 Position
0.69444	788-789	819-820
2.08333	773-774	819-820
2.08333	786-787	830-831
4.16667	774-746	819-820
4.16667	785-786	819-820
4.16667	801-802	818-829
4.16667	807-808	831-832
6.25000	789-790	819-820
6.25000	790-791	819-820
6.25000	790-791	831-832
6.25000	804-805	821-822
6.25000	918-919	833-834
8.33333	772-773	832-833
8.33333	780-781	819-820
8.33333	781-782	819-820
8.33333	782-783	819-820
8.33333	783-784	821-822
8.33333	786-787	822-823
8.33333	807-808	823-824
8.33333	966-967	821-822
10.4167	767-768	819-820
10.4167	770-771	819-820
10.4167	772-773	820-821
10.4167	772-773	821-822
10.4167	772-773	831-832
10.4167	775-776	823-824
10.4167	777-778	831-832
10.4167	782-783	830-831
10.4167	800-801	822-823
10.4167	920-921	833-834
10.4167	924-925	833-834
12.5000	761-762	819-820
12.5000	765-766	816-817
12.5000	768-769	833-834
12.5000	769-770	821-822
12.5000	769-770	831-832
12.5000	769-770	832-833

Appendix 2.2: Optimum MWs for maximum separation of clear mean from cloudy threshold

Number of SDs	MW1 Position	MW2 Position
1.97184	773 – 774	819 – 820
1.76347	785 – 786	819 – 820
1.71971	774 – 775	819 – 820
1.68737	807 – 808	831 – 832
1.59291	788 – 789	819 – 820
1.55883	786 – 787	822 – 823
1.48442	772 – 773	831 – 832
1.44269	918 – 919	833 – 834
1.41233	769 – 770	831 – 832
1.37221	800 – 801	822 – 823
1.37074	920 – 921	833 – 834
1.34497	765 – 766	822 – 823
1.32897	786 – 787	830 – 831
1.30568	790 – 791	819 – 820
1.28857	767 – 678	819 – 820
1.28330	782 – 783	819 – 820
1.27588	771 – 772	819 – 820
1.26493	782 – 783	822 – 823
1.26314	789 – 790	819 – 820
1.26055	780 – 781	822 – 823
1.25321	772 – 773	832 – 833
1.25219	780 – 781	819 – 820
1.24879	770 – 771	819 – 820
1.24846	807 – 808	823 – 824
1.24783	775 – 776	831 – 832
1.23818	773 – 774	822 – 823
1.21401	777 – 778	831 – 832
1.20116	924 – 925	833 – 834
1.19317	768 – 769	831 – 832
1.19248	767 – 768	831 – 832
1.18695	931 – 932	833 – 834
1.17907	783 – 784	822 – 823
1.17547	768 – 769	833 – 834
1.16089	919 – 920	833 – 834
1.16030	921 – 922	833 – 834
1.15978	770 – 771	831 – 832
1.13214	759 – 760	822 – 823

Appendix 2.3: Optimum MWs for greatest separation of clear mean from cloudy mean

Number of SD sums	MW1 Position	MW2 Position
1.58446	756 – 757	819 – 820
1.53686	760 – 761	819 – 820
1.51639	771 – 772	819 – 820
1.50570	755 – 756	819 – 820
1.49415	763 – 764	819 – 820
1.47820	764 – 765	819 – 820
1.47151	755 – 756	831 – 832
1.46617	749 – 750	819 – 820
1.46462	752 – 753	819 – 820
1.45618	757 – 758	819 – 820
1.45188	751 – 752	819 – 820
1.45157	750 – 751	819 – 820
1.44442	753 – 754	819 – 820
1.43934	760 – 761	822 – 823
1.43330	755 – 756	822 – 823
1.43284	760 – 761	831 – 832
1.43189	753 – 754	831 – 832
1.43058	748 – 749	819 – 820
1.42989	758 – 759	831 – 832
1.42731	770 – 771	819 – 820
1.42083	767 – 768	819 – 820
1.42022	754 – 755	819 – 820
1.41357	746 – 747	819 – 820
1.41110	756 – 757	831 – 832
1.41109	747 – 748	831 – 832
1.41096	747 – 748	819 – 820
1.40888	753 – 754	822 – 823
1.40608	745 – 746	819 – 820
1.40512	758 – 759	822 – 823
1.40459	761 – 762	819 – 820
1.40224	778 – 779	819 – 820
1.40062	744 – 745	819 – 820
1.39931	752 – 753	831 – 832
1.39642	752 – 753	822 – 823
1.38671	791 – 792	819 – 820
1.38232	747 – 748	822 – 823
1.37926	756 – 757	822 – 823

Appendix 3.1: Simulated Annealing trials retaining sequential alteration of MW boundaries

1. Initial Boundaries = 788 – 796 and 832 – 834
Constant ('const') = 0.5
Starting Temperature = 0.8
Temperature multiplied by factor = 0.8
After number of acceptances = 12
Or number of tries = 20
Multiplication factor for step sizes = 25
RESULT: RMSE = 0.18033307
Boundaries = 778.125 – 795.325 and 831.95 – 833.675
Final temperature = $5.44452 * 10^{-5}$
Randomu seeds of 4 and 5 respectively

2. Initial Boundaries = 774 – 777 and 830 – 833
Constant = 1
Starting Temperature = 0.05
Temperature multiplied by factor = 0.9
After number of acceptances = 4
Or number of tries = 8
Multiplication factor for step sizes = 600
RESULT: RMSE = 0.17708166
Boundaries =773.5 – 777.05 and 829.975 – 832.975
Final temperature = 0.00101378
Randomu Seeds of 1 and 4 respectively

3. Initial Boundaries = 774 – 775 and 819 – 820
Constant = 0.1
Starting Temperature = 2
Temperature multiplied by factor = 0.95
After number of acceptances = 10
Or number of tries = 20
Multiplication factor for step sizes = 20
RESULT: RMSE = 0.18194
Boundaries = 772.6 – 778.175 and 817.425 – 824.1
Final temperature = 0.3681

4. Initial Boundaries = 774 – 776 and 826 – 828
Constant = 1.5
Starting Temperature = 0.04
Temperature multiplied by factor = 0.85
After number of acceptances = 10
Or number of tries = 15
Multiplication factor for step sizes = 600
RESULT: RMSE = 0.24381685
Boundaries = 773.55 – 776.425 and 825.675 – 826.65
Final temperature = 0.00182398
Randomu seeds of 2 and 3 respectively

5. Initial Boundaries = 759 – 761 and 820 – 822
Constant = 2.5
Starting Temperature = 0.5
Temperature multiplied by factor = 0.7
After number of acceptances = 5
Or number of tries = 10
Multiplication factor for step sizes = 50
RESULT: RMSE = 0.19334114
Boundaries = 759.125 – 760.8 and 818.95 – 821.625
Final temperature = $2.70585 * 10^{-6}$
Randomu seeds of 3 and 4 respectively

6. Initial Boundaries = 773.75 – 775.25 and 818.75 – 820.25
Constant = 0.01
Starting Temperature = 1
Temperature multiplied by factor = 0.95
After number of acceptances = 8
Or number of tries = 12
Multiplication factor for step sizes = 275
RESULT: Error due to an upper microwindow boundary falling below a lower one

Appendix 3.2: Simulated Annealing trials by varying centre and width of both MWs

1. Initial Boundaries = 774 – 775 and 819 – 820
Constant = 0.5
Starting Temperature = 0.1
Temperature multiplied by factor = 0.95
After number of acceptances = 5
Or number of tries = 12
Multiplication factor for mean steps = 80
Multiplication factor for width changes = 40
RESULT: RMSE = 0.18709186
Boundaries = 774.675 – 777.425 and 819.9 – 822.475
Final temperature = 0.18709186
Randomu seeds of 1,2,3,4,5,6,7

2. Initial Boundaries = 790 – 793 and 818.5 – 821.5
Constant = 0.01
Starting Temperature = 0.2
Temperature multiplied by factor = 0.9
After number of acceptances = 5
Or number of tries = 12
Multiplication factor for mean steps = 100
Multiplication factor for width changes = 50
RESULT: RMSE = 0.22989429
Boundaries = 789.875 – 792.875 and 818.775 – 822.025
Final temperature = 0.2
Randomu Seeds of 11,12,13,14,15,16,17

3. Initial Boundaries = 790 – 793 and 830 – 833
Constant = 0.3
Starting Temperature = 0.2
Temperature multiplied by factor = 0.9
After number of acceptances = 5
Or number of tries = 12
Multiplication factor for mean steps = 100
Multiplication factor for width changes = 75
RESULT: RMSE = 0.23719820
Boundaries = 778.875 – 795.375 and 830.775 – 836.025
Final temperature = 0.0129222
Randomu Seeds of 111,112,113,114,115,116,117

4. Initial Boundaries = 749 – 751 and 849 – 851
Constant = 0.1
Starting Temperature = 0.1
Temperature multiplied by factor = 0.9
After number of acceptances = 5
Or number of tries = 12
Multiplication factor for mean steps = 150
Multiplication factor for width changes = 100
RESULT: RMSE = 0.69728274
Boundaries = 749.525 – 753.375 and 848.575 – 852.825
Final temperature = $1.54452 * 10^{-7}$
Randomu Seeds of 1111,1112,1113,1114,1115,1116,1117

5. Initial Boundaries = 775 - 776 and 805 - 815
Constant = 0.02
Starting Temperature = 1
Temperature multiplied by factor = 0.75
After number of acceptances = 8
Or number of tries = 15
Multiplication factor for mean steps = 25
Multiplication factor for width changes = 10
RESULT: RMSE = 0.41522466
      Boundaries = 754.875 - 756.625 and 806.6 - 813.85
      Final temperature = 0.133484
Randomu Seeds of 11111,11112,11113,11114,11115,11116,11117

6. Initial Boundaries = 785 - 786 and 819 - 820
Constant = 0.005
Starting Temperature = 2
Temperature multiplied by factor = 0.9
After number of acceptances = 7
Or number of tries = 15
Multiplication factor for mean steps = 5
Multiplication factor for width changes = 5
RESULT: RMSE = 0.25589121
      Boundaries = 783.825 - 784.525 and 819.15 - 820.25
      Final temperature = 1.8
Randomu Seeds of 111111,111112,111113,111114,111115,111116,111117

Appendix 4: Programs

Note: The operational components of the code are interspersed with commentary (designated by a semicolon) which aims to explain my intentions where elucidation is deemed necessary.

Appendix 4.1: Calculation of CI and CEF for initial MWs

```
;Define the arrays that will be used

th_arrstr = ['06000','09000','12000','15000','18000','21000']
th_arr = [6,9,12,15,18,21]
;This is the tangent height of the simulated spectrum.

atm_arr =
['ngt','equ','win','sum','ngt_var','equ_var','win_var','sum_var']
;Atmosphere type ('var' = variation)

kext_arrstr = ['0.001','0.01','0.1']
kext_arr = [0.001,0.01,0.1]
;Extinction coefficient

CT_arrstr = ['-2.0','-1.5','-1.0','-0.5','0.0','0.5','1.0','1.5','2.0']
CT_arr = [-2.0,-1.5,-1.0,-0.5,0,0.5,1.0,1.5,2.0]
;Displacement of cloud top from tangent height

n =
n_elements(th_arrstr)*n_elements(atm_arr)*n_elements(kext_arrstr)*n_eleme
nts(CT_arrstr)
;This is the total number of permutations of these parameters, and equals
the number of simulated spectra (1296).

Atm = strarr (n)
Alt  = fltarr (n)
Ext = fltarr (n)
Height = fltarr (n)
;These will allow identification of the value of a specific parameter for
any one of the 1296 spectra.

CI_arr = fltarr (n)
CEF_arr = fltarr(n)

meanrad1_sim = fltarr(n)
meanrad2_sim = fltarr(n)

;Now, bring in the tangent point (z) values and corresponding convolution
(psi) values into the arrays z_fov and psi_fov.

nptfov = 401
openr,lun,'Trapezium_fine.asc',/get_lun
z_fov = fltarr(nptfov)
psi_fov = fltarr(nptfov)
readf,lun,z_fov,psi_fov
free_lun, lun
psi_fov = psi_fov/total(psi_fov)
```

```
;Define all constants/variables

Re = 6367.421         ;This is the radius of the Earth
index = 0

;Loop over Ext, CTH, TH and Atm type.

for l = 0,n_elements(th_arr)-1 do begin
     for k = 0,n_elements(kext_arr)-1 do begin
          for j = 0,n_elements(CT_arr)-1 do begin
               for i = 0,n_elements(atm_arr)-1 do begin

;First, must distinguish between the loading in of clear or cloudy
spectra as they have slightly different file names. If the CTH is -2.0, a
spectrum is clear. Read in the spectrum.

if CT_arr(j) ne -2.0 then begin

     str =
     atm_arr(i)+'_'+CT_arrstr(j)+'_'+kext_arrstr(k)+'_'+th_arrstr(l)

     rfmrd,'/home/jupiter/eodg/hurley/janeRFM/$
     rad_cloudy_CFCs_'+str+'.asc',W,r

endif else begin

     str = atm_arr(i)+'_nopert'+th_arrstr(l)

     rfmrd,'/home/jupiter/eodg/hurley/janeRFM/$
     rad_clearA_CFCs_'+str+'.asc',W,r

endelse

;Calculate the CI. This is done by first finding the two MW boundaries,
then finding the mean radiance within them, before finally taking their
ratio. The CI value for each of the 1296 spectra is stored in the array
CI_arr.

minval = min(abs(W-788.0),locmin_MW1_1)
minval = min(abs(W-796.0),locmin_MW1_2)
minval = min(abs(W-832.0),locmin_MW2_1)
minval = min(abs(W-834.0),locmin_MW2_2)

mean_rad_MW1 = mean(r(locmin_MW1_1:locmin_MW1_2))
mean_rad_MW2 = mean(r(locmin_MW2_1:locmin_MW2_2))

meanrad1_sim(index) = mean_rad_MW1
meanrad2_sim(index) = mean_rad_MW2

CI = mean_rad_MW1 / mean_rad_MW2

CI_arr(index) = CI

;Now, calculate the CEF.

CEF = 0

;For every z value between the bottom of the FOV and the CTH, calculate
```

```
the path length of the incident light beam, and then sum the numerator of
the CEF expression. The denominator may be neglected as it equals one.
Store the CEF value in CEF_arr.

for i_z = 0,((2.0 + CT_arr(j))*100.0) - 1 do begin

      x = sqrt((Re + th_arr(l) + CT_arr(j))^2 - (Re + th_arr(l) +
      z_fov(i_z))^2)

      y = (1. - exp(-kext_arr(k)*x))*psi_fov(i_z)

      CEF = CEF + y

endfor

CEF_arr(index) = CEF

Atm(index) = atm_arr(i)
Alt(index) = CT_arrstr(j)
Ext(index) = kext_arrstr(k)
Height(index) = th_arrstr(l)

index = index + 1

endfor
endfor
endfor
endfor

set_plot,'ps'
device,filename = 'CI_vs_CEF.ps'

plot, CI_arr,CEF_arr, yrange = [-0.1,1.1], ystyle = 1, $
xrange = [0,13], xstyle = 1, $
title = 'Relationship between CEF and CI for initial MWs', $
xtitle = 'CI', ytitle = 'CEF', linestyle = 0, psym = 1

device,/close

;The relationship between CI and CEF for these initial MWs may be
plotted.

save,CI_arr,CEF_arr,Atm,Alt,Ext,Height,meanrad1_sim,meanrad2_sim,filename
= 'CI+CEF_Results_2.sav'

;All arrays are saved for future reference.

end
```

Appendix 4.2: Calculation of best fit line parameters and RMSE for initial MWs

```
;First, the arrays created in the previous program are restored, if
necessary.

restore,'CI+CEF_Results_2.sav'

n_spec = 1296         ;This constant is defined as the number of spectra.

log_CI_arr = fltarr(n_spec)
log_CEF_arr = fltarr(n_spec)

sort_CI = fltarr(n_spec)
sort_CEF = fltarr(n_spec)

lad_arr_sim = fltarr(2)
;This array stores the A (y-intercept) and B (gradient) parameters of the
best fit line, which is yet to be calculated.

rec_mr1_sqrd = 1/(meanrad1_sim)^2
rec_mr2_sqrd = 1/(meanrad2_sim)^2
;These will be useful in the noise calculation.

c1 = 25 / sqrt(321)
c2 = 25 / sqrt(81)
c12 = c1 ^ 2
c22 = c2 ^ 2

;These represent the noise associated with each mean radiance. c1 is for
MW1, which has width 8 (or 8 * 40 + 1 = 321 spectral points), and c2 for
MW2, which has width 2 (2 * 40 + 1 = 81).

RMSE_sum = 0

for i = 0,n_spec-1 do begin

      log_CI_arr(i) = alog10(CI_arr(i))

      if CEF_arr(j) eq 0 then begin

            log_CEF_arr(j) = -2.5

      endif else begin

            log_CEF_arr(j) = alog10(CEF_arr(j))

      endelse

endfor

;This generates arrays storing the log (to the base 10) of the CI and CEF
values, respectively. When the CEF is 0, log(CEF) is set to -2.5 (as this
seems to conform to the straight line fit for the rest of the points).

sort_CI = log_CI_arr(sort(log_CI_arr))
sort_CEF = log_CEF_arr(sort(log_CI_arr))
```

```
;Sorting the arrays into ascending order facilitates the ladfit
procedure.

lad_arr_sim(*) = ladfit(sort_CI, sort_CEF)

A = lad_arr_sim(0)
B = lad_arr_sim(1)
B2 = B^2

for k = 0,n_spec - 1 do RMSE_sum = RMSE_sum + $
     ( log_CEF_arr (k) - (A + B*log_CI_arr(k)))^2 + $
     1/(alog(10))^2 * (c12 * rec_mr1_sqrd(k) + c22 * rec_mr2_sqrd(k))*B2

print,sqrt(RMSE_sum/n_spec)          ;This is the RMSE

save,log_CEF_arr,filename = 'logCEF.sav'

;This array will be integral to all future RMSE calculations

end
```

Appendix 4.3: Calculation of CI using each potential combination of MWs of width 1 wavenumber in the A band

```
;Define the same arrays as before, which represent the atmospheric
permutations.

th_arrstr = ['06000','09000','12000','15000','18000','21000']
th_arr = [6,9,12,15,18,21]
;Tangent height

atm_arr =
['ngt','equ','win','sum','ngt_var','equ_var','win_var','sum_var']
;Atmosphere type

kext_arrstr = ['0.001','0.01','0.1']
kext_arr = [0.001,0.01,0.1]
;Extinction coefficient

CT_arrstr = ['-2.0','-1.5','-1.0','-0.5','0.0','0.5','1.0','1.5','2.0']
CT_arr = [-2.0,-1.5,-1.0,-0.5,0,0.5,1.0,1.5,2.0]
;Displacement of cloud top from tangent height

n =
n_elements(th_arrstr)*n_elements(atm_arr)*n_elements(kext_arrstr)*n_eleme
nts(CT_arrstr)

Atm = strarr (n)
Alt  = strarr (n)
Ext = strarr (n)
Height = strarr (n)
CI_arr = fltarr (n)

;The following arrays are two-dimensional. The first dimension represent
which of the 81225 1 wavenumber wide MW combinations is being dealt with,
and the second pertains to which particular permutation of the
atmospheric constants is being used.

CI_a = fltarr(81225,n)

meanrad1 = fltarr(81225,n)
meanrad2 = fltarr(81225,n)

mw1_arr = fltarr(81225)
mw2_arr = fltarr(81225)
;These will store the lower bound of MW1 and MW2 respectively for each MW
combination for reference.

nmw = 970 - 685       ;This is the width of the A band

meanrad = fltarr(nmw)

index = 0

;Loop over permutations

for l = 0,n_elements(th_arr)-1 do begin
     for k = 0,n_elements(kext_arr)-1 do begin
```

```
           for j = 0,n_elements(CT_arr)-1 do begin
                for i = 0,n_elements(atm_arr)-1 do begin

;Differentiate between the loading in of clear or cloudy spectra
depending on whether the CTH is -2 or not.

if CT_arr(j) ne -2.0 then begin

     str =
     atm_arr(i)+'_'+CT_arrstr(j)+'_'+kext_arrstr(k)+'_'+th_arrstr(l)

     rfmrd,'/home/jupiter/eodg/hurley/janeRFM$
     /rad_cloudy_CFCs_'+str+'.asc',W,r

endif else begin

     str = atm_arr(i)+'_nopert'+th_arrstr(l)

     rfmrd,'/home/jupiter/eodg/hurley/janeRFM$
     /rad_clearA_CFCs_'+str+'.asc',W,r

endelse

;Now, define the microwindow positions

counterindex = long(0)

for y = 0,nmw - 1 do begin

     locmin1 = 40L * y

     locmin2 = locmin1 + 40

     meanrad(y) = mean(r(locmin1:locmin2))

;This stores the mean radiance in every potential 1 wide MW in the A
band.

endfor

for i_mw = 0,nmw-1 do begin

     for j_mw = 0,nmw-1 do begin

           CI_a(counterindex,index) = meanrad[i_mw]/meanrad[j_mw]

;Meanrad1 and 2 store the mean radiances used for the 2 microwindows, for
each particular case of microwindow combination, and spectrum used.

           meanrad1(counterindex,index) = meanrad(i_mw)
           meanrad2(counterindex,index) = meanrad(j_mw)

           mw1_arr(counterindex) = 685 + i_mw
           mw2_arr(counterindex) = 685 + j_mw

           print,index,'  ',counterindex
;This allows easy identification of the program's progress
```

```
            counterindex = counterindex + 1

      endfor

endfor

Atm(index) = atm_arr(i)
Alt(index) = CT_arrstr(j)
Ext(index) = kext_arrstr(k)
Height(index) = th_arrstr(l)

index = index + 1

endfor
endfor
endfor
endfor

save,meanrad1,meanrad2,Alt,CI_a,filename = 'Smooth_Results.sav'

save,mw1_arr,mw2_arr,filename = 'Reference1.sav'

save,Atm,Alt,Ext,Height,filename = 'Reference2.sav'

end
```

Appendix 4.4: Calculation of line parameters and RMSE for each set of CI values

```
;Define constants. 'noise' is the noise value associated with each
spectral point; n_pts is the number of spectral points within each MW
(1 * 40 + 1 = 41).

noise = 25.0
n_pts = 41

c2 = noise^2 / n_pts
a = (alog(10))^2

;Restore meanrad1 & 2, CI_a and log_CEF_arr.

restore,'Smooth_Results.sav'
restore,'logCEF.sav'

n_spec = n_elements(log_CEF_arr)      ;Number of spectra
n_pairs = n_elements(CI_a)/n_spec     ;Number of MW combinations

imr1 = 1.0/meanrad1^2
imr2 = 1.0/meanrad2^2

lad_arr = fltarr(n_pairs,2)
RMSE_mod = fltarr(n_pairs)

;For each microwindow combination, calculate the ladfit line parameters,
storing them in lad_arr.

for x = 0L,n_pairs - 1 do begin

     LOGCIA = alog10 (CI_a[x,*])
     lad_arr(x,*) = ladfit(LOGCIA,log_CEF_arr)

;x must be a long variable type as integers cannot reach 81225.

;for each combination, find the total RMSE by summing the squares of the
uncertainty from the line and the noise for each spectrum type
(represented by points on graph).

     RMSE_sum = 0.0D0

;RMSE_sum is made double-precision, to reduce information loss.

     A = lad_arr(x,0)
     B = lad_arr(x,1)

;These are the ladfit line parameters.

     B2 = B ^ 2

     for k = 0,n_spec - 1 do RMSE_sum = RMSE_sum + $
          (log_CEF_arr(k) - (A + B * LOGCIA(K)))^2 + $
          (c2/a)*(imr1[x,k] + imr2[x,k]) * B2

;Store the square root of the mean of this value in the array RMSE_mod.
```

```
      RMSE_mod(x) = sqrt(RMSE_sum/n_spec)
      print,x
endfor
save,RMSE_mod,filename = 'RMSE_mod.sav'
end
```

Appendix 4.5: Iterative procedure whereby MW bounds changed by 0.025cm^{-1} per iteration

```
;This is an iteration program streamlined for changing the boundaries by
1 point each iteration. The more advanced programs to come are based on a
different blueprint.

;The MW boundaries are set at the beginning (both the actual spectral
point values and the wavenumber boundaries).

mw1_l = 788.0 & locmin_mw1_l = long((mw1_l - 685.0) * 40 + 0.001)
mw1_u = 796.0 & locmin_mw1_u = long((mw1_u - 685.0) * 40 + 0.001)
mw2_l = 832.0 & locmin_mw2_l = long((mw2_l - 685.0) * 40 + 0.001)
mw2_u = 834.0 & locmin_mw2_u = long((mw2_u - 685.0) * 40 + 0.001)

;Define atmospheric permutation arrays, as before.

th_arrstr = ['06000','09000','12000','15000','18000','21000']
th_arr = [6,9,12,15,18,21]
;Tangent height

atm_arr =
['ngt','equ','win','sum','ngt_var','equ_var','win_var','sum_var']
;Atmosphere type

kext_arrstr = ['0.001','0.01','0.1']
kext_arr = [0.001,0.01,0.1]
;Extinction coefficient

CT_arrstr = ['-2.0','-1.5','-1.0','-0.5','0.0','0.5','1.0','1.5','2.0']
CT_arr = [-2.0,-1.5,-1.0,-0.5,0,0.5,1.0,1.5,2.0]
;Displacement of cloud top from tangent height

n_spec =
n_elements(th_arrstr)*n_elements(atm_arr)*n_elements(kext_arrstr)*n_eleme
nts(CT_arrstr)

n_perm = 9
;This is the number of boundary changes tried each iteration.

CI_arr = dblarr(n_perm,n_spec)

meanrad1 = dblarr(n_perm,n_spec)
meanrad2 = dblarr(n_perm,n_spec)

;The elements of these arrays are double-precision

p = 1 / alog(10)^2

RMSE = dblarr(n_perm)

width_mw1 = fltarr(n_perm)
width_mw2 = fltarr(n_perm)

lad_arr = fltarr(n_perm,2)
```

```
;All of these arrays are overwritten during consecutive iterations.

noise2 = 25.0 ^ 2

;Restore log_CEF_arr
restore,'logCEF.sav'

change = 1     ;Used to determine whether another iteration is performed
z = 0
niter = 0
;The value of 'niter' is the number of iterations already performed

while change do begin

ispec = 0

npt1 = locmin_mw1_u - locmin_mw1_l + 1
npt2 = locmin_mw2_u - locmin_mw2_l + 1

;These are constants telling you how many spectral points there are in
mw1 and mw2

width_mw1 = float ( npt1 + [ 0, 1, -1, -1, 1, 0, 0, 0, 0 ] )
width_mw2 = float ( npt2 + [ 0, 0, 0, 0, 0, 1, -1, -1, 1 ] )

;Load in the spectra.

for l = 0,n_elements(th_arr)-1 do begin
      for k = 0,n_elements(kext_arr)-1 do begin
         for j = 0,n_elements(CT_arr)-1 do begin
           for i = 0,n_elements(atm_arr)-1 do begin

if j eq 0 then begin

      str = atm_arr(i)+'_nopert'+th_arrstr(l)

      rfmrd,'/home/jupiter/eodg/hurley/janeRFM$
      /rad_clearA_CFCs_'+str+'.asc',W,r

endif else begin

      str = atm_arr(i)+'_' +CT_arrstr(j)+'_'+kext_arrstr(k)+$
      '_'+th_arrstr(l)

      rfmrd,'/home/jupiter/eodg/hurley/janeRFM$
      /rad_cloudy_CFCs_'+str+'.asc',W,r

endelse

      mw1tot = total (r[locmin_mw1_l:locmin_mw1_u])
      mw2tot = total (r[locmin_mw2_l:locmin_mw2_u])

;These variables store the total of the radiance values of all spectral
points within each MW. The mean radiance is therefore this value divided
by the number of radiance values summed.

      meanrad1[0,ispec] = mw1tot / npt1
```

```
      meanrad1[1,ispec] = ( mw1tot + r[locmin_mw1_u+1] )/ ( npt1 + 1 )
      meanrad1[2,ispec] = ( mw1tot - r[locmin_mw1_u] )/ ( npt1 - 1 )
      meanrad1[3,ispec] = ( mw1tot - r[locmin_mw1_l] )/ ( npt1 - 1 )
      meanrad1[4,ispec] = ( mw1tot + r[locmin_mw1_l-1] )/ ( npt1 + 1 )
      meanrad1[5:8,ispec] = meanrad1[0,ispec]

      meanrad2[0,ispec] = mw2tot / npt2

      meanrad2[1:5,ispec] = meanrad2[0,ispec]
      meanrad2[5,ispec] = ( mw2tot + r[locmin_mw2_u + 1] ) / ( npt2 + 1 )
      meanrad2[6,ispec] = ( mw2tot - r[locmin_mw2_u] )/ ( npt2 - 1 )
      meanrad2[7,ispec] = ( mw2tot - r[locmin_mw2_l] )/ ( npt2 - 1 )
      meanrad2[8,ispec] = ( mw2tot + r[locmin_mw2_l - 1] ) / ( npt2 + 1 )

;These define the meanrad values associated with each of the 9 changes
made during each iteration. For example, permutation '1' results in the
inclusion of an additional point that is adjacent to the upper bound of
MW1. Hence the total has this radiance value added to it, and it is
divided by npt + 1.

      CI_arr(*,ispec) = meanrad1(*,ispec) / meanrad2(*,ispec)

      ispec = ispec + 1

endfor
endfor
endfor
endfor

;Now we have a full set of cloud index values for each of the 9
possibilities above. Now, calculate ladfit parameters and RMSE for each.

imr1 = 1/meanrad1^2
imr2 = 1/meanrad2^2

for y = 0,n_perm - 1 do begin

      RMSE_sum = 0.0D0

      lad_arr(y,*) = ladfit (alog10(CI_arr(y,*)),log_CEF_arr(*))

      A = lad_arr(y,0)
      B = lad_arr(y,1)
      B2 = B^2

      for i = 0,n_spec - 1 do RMSE_sum = RMSE_sum $
            + (log_CEF_arr(i) - (A + B*alog10(CI_arr(y,i))))^2 $
            + p*B2*(((noise2/width_mw1(y)) * imr1(y,i)) $
            + ((noise2/width_mw2(y)) * imr2(y,i)))

      RMSE(y) = sqrt(RMSE_sum / n_spec)

;RMSE stores the RMSE values for each of the 9 changes tried each
iteration.

endfor

;The 0th 'change' was in fact no change, so it is this value that must be
```

```
bettered by one of the consecutive 8 for the iteration to continue.

if z eq 0 then print,'Initial RMSE =', RMSE(0)

;z merely defines whether the current iteration is the first iteration or
not. If it is, z eq 0 and the initial RMSE is also printed.

best = min (RMSE, ibest)

;'ibest' is a variable whose value is the element number in RMSE that
gave the lowest RMSE. We only continue if ibest is greater than 0.

if ibest gt 0 then begin

;The locmin values are changed according to which of the 8 changes gave
the lowest RMSE.

  case ibest of

      1: locmin_mw1_u = locmin_mw1_u + 1
      2: locmin_mw1_u = locmin_mw1_u - 1
      3: locmin_mw1_l = locmin_mw1_l + 1
      4: locmin_mw1_l = locmin_mw1_l - 1
      5: locmin_mw2_u = locmin_mw2_u + 1
      6: locmin_mw2_u = locmin_mw2_u - 1
      7: locmin_mw2_l = locmin_mw2_l + 1
      8: locmin_mw2_l = locmin_mw2_l - 1

  endcase

      print, 'No. Iterations =', niter
      niter = niter + 1

      print, locmin_mw1_l,locmin_mw1_u,locmin_mw2_l,locmin_mw2_u

      print, 'Best =', Best
      z = 1

endif else begin

      print,'Lowest RMSE =',Best,' ',locmin_mw1_l,' -',locmin_mw1_u,$
      '  ',locmin_mw2_l,' -',locmin_mw2_u

      print,'number of iterations equals:', niter - 1

      change = 0

      z = 1

;The program ends if the current RMSE cannot be bettered (change becomes
0).

endelse

endwhile

end
```

Appendix 4.6: Iterative procedure whereby bound changes are user-defined

```
th_arrstr = ['06000','09000','12000','15000','18000','21000']
th_arr = [6,9,12,15,18,21]
;Tangent height

atm_arr =
['ngt','equ','win','sum','ngt_var','equ_var','win_var','sum_var']
;Atmosphere type

kext_arrstr = ['0.001','0.01','0.1']
kext_arr = [0.001,0.01,0.1]
;Extinction coefficient

CT_arrstr = ['-2.0','-1.5','-1.0','-0.5','0.0','0.5','1.0','1.5','2.0']
CT_arr = [-2.0,-1.5,-1.0,-0.5,0,0.5,1.0,1.5,2.0]
;Displacement of cloud top from tangent height

n_spec =
n_elements(th_arrstr)*n_elements(atm_arr)*n_elements(kext_arrstr)*n_eleme
nts(CT_arrstr)
n_perm = 9

CI_arr = dblarr(n_perm,n_spec)

meanrad1 = dblarr(n_perm,n_spec)
meanrad2 = dblarr(n_perm,n_spec)

p = 1/alog(10)^2

RMSE = dblarr(n_perm)

width_mw1 = fltarr(n_perm)
width_mw2 = fltarr(n_perm)

lad_arr = fltarr(n_perm,2)

x = 0
z = 0

noise2 = 25.0 ^ 2

restore,'logCEF.sav'

;From now on, this program is significantly different to that located in
appendix 4.5.

n_steps = 7

for step = 0,n_steps - 1 do begin

case step of
  0: step_size = 50
  1: step_size = 35
  2: step_size = 20
  3: step_size = 10
  4: step_size = 5
```

```
  5: step_size = 3
  6: step_size = 1
endcase

;n_steps defines the number of times the step sizes will be changed,
whilst the case loop defines the size of the step changes for each level.

while x eq 0 do begin

index = 0

for l = 0,n_elements(th_arr)-1 do begin
     for k = 0,n_elements(kext_arr)-1 do begin
          for j = 0,n_elements(CT_arr)-1 do begin
               for i = 0,n_elements(atm_arr)-1 do begin

if CT_arr(j) ne -2.0 then begin

     str =
     atm_arr(i)+'_'+CT_arrstr(j)+'_'+kext_arrstr(k)+'_'+th_arrstr(l)

     rfmrd,'/home/jupiter/eodg/hurley/janeRFM$
     /rad_cloudy_CFCs_'+str+'.asc',W,r

endif else begin

     str = atm_arr(i)+'_nopert'+th_arrstr(l)

     rfmrd,'/home/jupiter/eodg/hurley/janeRFM$
     /rad_clearA_CFCs_'+str+'.asc',W,r

endelse

if z eq 0 then begin
     locmin_mw1_u = (777.0 - 685) * 40     ;Set the initial MW boundaries
     locmin_mw1_l = (773.0 - 685) * 40
     locmin_mw2_u = (822.0 - 685) * 40
     locmin_mw2_l = (820.5 - 685) * 40
endif else begin

if index eq 0 then begin

     if where (RMSE eq min(RMSE)) eq 1 then locmin_mw1_u = locmin_mw1_u
+ step_size
     if where (RMSE eq min(RMSE)) eq 2 then locmin_mw1_u = locmin_mw1_u
- step_size
     if where (RMSE eq min(RMSE)) eq 3 then locmin_mw1_l = locmin_mw1_l
+ step_size
     if where (RMSE eq min(RMSE)) eq 4 then locmin_mw1_l = locmin_mw1_l
- step_size

     if where (RMSE eq min(RMSE)) eq 5 then locmin_mw2_u = locmin_mw2_u
+ step_size
     if where (RMSE eq min(RMSE)) eq 6 then locmin_mw2_u = locmin_mw2_u
- step_size
     if where (RMSE eq min(RMSE)) eq 7 then locmin_mw2_l = locmin_mw2_l
+ step_size
     if where (RMSE eq min(RMSE)) eq 8 then locmin_mw2_l = locmin_mw2_l
```

```
- step_size

endif

;These define the change in MW boundaries according to which of the 8
changes in the previous iteration gave the best result.

endelse

for y = 0,n_perm - 1 do begin

      If y eq 1 then locmin_mw1_u = locmin_mw1_u + step_size
      If y eq 2 then locmin_mw1_u = locmin_mw1_u - step_size
      If y eq 3 then locmin_mw1_l = locmin_mw1_l + step_size
      If y eq 4 then locmin_mw1_l = locmin_mw1_l - step_size

      If y eq 5 then locmin_mw2_u = locmin_mw2_u + step_size
      If y eq 6 then locmin_mw2_u = locmin_mw2_u - step_size
      If y eq 7 then locmin_mw2_l = locmin_mw2_l + step_size
      If y eq 8 then locmin_mw2_l = locmin_mw2_l - step_size

;These define the eight changes which will be tested for every iteration.

width_mw1(y) = locmin_mw1_u - locmin_mw1_l + 1
width_mw2(y) = locmin_mw2_u - locmin_mw2_l + 1

;These define the width of the MWs.

meanrad1(y,index) = mean(r(locmin_mw1_l:locmin_mw1_u))
meanrad2(y,index) = mean(r(locmin_mw2_l:locmin_mw2_u))

CI_arr(y,index) = meanrad1(y,index)/meanrad2(y,index)

      If y eq 1 then locmin_mw1_u = locmin_mw1_u - step_size
      If y eq 2 then locmin_mw1_u = locmin_mw1_u + step_size
      If y eq 3 then locmin_mw1_l = locmin_mw1_l - step_size
      If y eq 4 then locmin_mw1_l = locmin_mw1_l + step_size

      If y eq 5 then locmin_mw2_u = locmin_mw2_u - step_size
      If y eq 6 then locmin_mw2_u = locmin_mw2_u + step_size
      If y eq 7 then locmin_mw2_l = locmin_mw2_l - step_size
      If y eq 8 then locmin_mw2_l = locmin_mw2_l + step_size

;These change the boundaries back to the way they were at the beginning
of the current iteration.

endfor     ;This is for the 8 boundary changes

index = index + 1

endfor
endfor
endfor
endfor     ;These are for the spectral loops.

imr1 = 1/meanrad1^2
imr2 = 1/meanrad2^2
```

```
for y = 0,n_perm - 1 do begin

      RMSE_sum = 0.0D0

      lad_arr(y,*) = ladfit(alog10(CI_arr(y,*)),log_CEF_arr(*))

      A = lad_arr(y,0)
      B = lad_arr(y,1)
      B2 = B^2

      for i = 0,n_spec - 1 do RMSE_sum = RMSE_sum $
            + (log_CEF_arr(i) - (A + B*alog10(CI_arr(y,i))))^2 $
            + p * B2 * (((noise2/width_mw1(y)) * imr1(y,i)) $
            + ((noise2/width_mw2(y)) * imr2(y,i)))

      RMSE(y) = sqrt(RMSE_sum/n_spec)

endfor

if z eq 0 then begin
   Best = RMSE(0)
   print,'Initial RMSE =',Best
endif

;This tells you what the initial RMSE value is, for the defined MW
positions before any changes.

if min(RMSE) lt Best then begin

      Best = min(RMSE)
      x = 0

      print,z

      print,Best

      print,'Step size =',step_size

endif else begin

      x = 1
      print,'Lowest RMSE =',Best,'  ',locmin_mw1_l,' ',locmin_mw1_u, $
      '  ',locmin_mw2_l,' ',locmin_mw2_u
      print,'number of iterations equals:',z

;Setting x to 1 means the while loop is no longer satisfied, so the
program will terminate.

endelse

z = z + 1

endwhile

x = 0

endfor
end
```

Appendix 4.7: Simulated Annealing - MW bounds changed sequentially

```
;Note that the values of many variables in this and the following program
merely reflect the last time that the programs were run - they can be
changed freely.

locmin_mw1_u = (796.0 - 685) * 40
locmin_mw1_l = (788.0 - 685) * 40
locmin_mw2_u = (834.0 - 685) * 40
locmin_mw2_l = (832.0 - 685) * 40

th_arrstr = ['06000','09000','12000','15000','18000','21000']
th_arr = [6,9,12,15,18,21]
;Tangent height

atm_arr =
['ngt','equ','win','sum','ngt_var','equ_var','win_var','sum_var']
;Atmosphere type

kext_arrstr = ['0.001','0.01','0.1']
kext_arr = [0.001,0.01,0.1]
;Extinction coefficient

CT_arrstr = ['-2.0','-1.5','-1.0','-0.5','0.0','0.5','1.0','1.5','2.0']
CT_arr = [-2.0,-1.5,-1.0,-0.5,0,0.5,1.0,1.5,2.0]
;Displacement of cloud top from tangent height

n_spec =
n_elements(th_arrstr)*n_elements(atm_arr)*n_elements(kext_arrstr)*n_eleme
nts(CT_arrstr)

n_perm = 9

CI_arr = dblarr(n_perm,n_spec)

meanrad1 = dblarr(n_perm,n_spec)
meanrad2 = dblarr(n_perm,n_spec)

p = 1/alog(10)^2

RMSE = dblarr(n_perm)

width_mw1 = fltarr(n_perm)
width_mw2 = fltarr(n_perm)

lad_arr = fltarr(n_perm,2)

x = 0
z = 0

noise2 = 25.0 ^ 2

restore,'logCEF.sav'

;Define annealing constants
```

```
det = 0
;This will allow the program's position through the 8 changes to be
remembered, and thus the correct continuation to be resumed after RMSE
testing.

T = 0.8
;This is the initial 'temperature'

const = 0.5
;This is the constant in the probability of acceptance formula

n_pot = 0
n_acc = 0
;These define how many attempted changes or accepted changes,
respectively, elapse before the temperature is lowered.

seed_1 = 4
seed_2 = 5
;These are the 'seeds' required for the generation of random numbers

de = 0
;This will determine after how many consecutive rejected changes the
program ceases

while x eq 0 do begin

x = 1

if n_pot eq 20 then begin
   T = T * 0.8
   n_pot = 0
   n_acc = 0
endif

if n_acc eq 12 then begin
   T = T * 0.8
   n_pot = 0
   n_acc = 0
endif

print,'     ---'
print,'T is',T

ran = randomu(seed_1)

if ran * T * 25 + 0.5 lt 1 then step_size = 1 $
else step_size = fix(ran * T * 25 + 0.5)

;This defines the size of the MW bound changes to be tries each
iteration, and ensures that they never fall below 1.

print,'step_size is',step_size
index = 0

;Load in the spectra.

for l = 0,n_elements(th_arr)-1 do begin
```

```
      for k = 0,n_elements(kext_arr)-1 do begin
           for j = 0,n_elements(CT_arr)-1 do begin
                for i = 0,n_elements(atm_arr)-1 do begin

;Differentiate between the loading in of clear or cloudy spectra.

if CT_arr(j) ne -2.0 then begin

      str =
      atm_arr(i)+'_'+CT_arrstr(j)+'_'+kext_arrstr(k)+'_'+th_arrstr(l)

      rfmrd,'/home/jupiter/eodg/hurley/janeRFM$
      /rad_cloudy_CFCs_'+str+'.asc',W,r

endif else begin

      str = atm_arr(i)+'_nopert'+th_arrstr(l)

      rfmrd,'/home/jupiter/eodg/hurley/janeRFM$
      /rad_clearA_CFCs_'+str+'.asc',W,r

endelse

for y = det,n_perm - 1 do begin

      If y eq 1 then locmin_mw1_u = locmin_mw1_u + step_size
      If y eq 2 then locmin_mw1_u = locmin_mw1_u - step_size
      If y eq 3 then locmin_mw1_l = locmin_mw1_l + step_size
      If y eq 4 then locmin_mw1_l = locmin_mw1_l - step_size

      If y eq 5 then locmin_mw2_u = locmin_mw2_u + step_size
      If y eq 6 then locmin_mw2_u = locmin_mw2_u - step_size
      If y eq 7 then locmin_mw2_l = locmin_mw2_l + step_size
      If y eq 8 then locmin_mw2_l = locmin_mw2_l - step_size

width_mw1(y) = locmin_mw1_u - locmin_mw1_l + 1
width_mw2(y) = locmin_mw2_u - locmin_mw2_l + 1

meanrad1(y,index) = mean(r(locmin_mw1_l:locmin_mw1_u))
meanrad2(y,index) = mean(r(locmin_mw2_l:locmin_mw2_u))

CI_arr(y,index) = meanrad1(y,index)/meanrad2(y,index)

      If y eq 1 then locmin_mw1_u = locmin_mw1_u - step_size
      If y eq 2 then locmin_mw1_u = locmin_mw1_u + step_size
      If y eq 3 then locmin_mw1_l = locmin_mw1_l - step_size
      If y eq 4 then locmin_mw1_l = locmin_mw1_l + step_size

      If y eq 5 then locmin_mw2_u = locmin_mw2_u - step_size
      If y eq 6 then locmin_mw2_u = locmin_mw2_u + step_size
      If y eq 7 then locmin_mw2_l = locmin_mw2_l - step_size
      If y eq 8 then locmin_mw2_l = locmin_mw2_l + step_size

endfor

index = index + 1

endfor
```

```
endfor
endfor
endfor     ;These are for the spectral permutation loops

imr1 = 1/meanrad1^2
imr2 = 1/meanrad2^2

change = 0

for y = det,n_perm - 1 do begin

      RMSE_sum = 0.0D0

      lad_arr(y,*) = ladfit(alog10(CI_arr(y,*)),log_CEF_arr(*))

      A = lad_arr(y,0)
      B = lad_arr(y,1)
      B2 = B^2

      for i = 0,n_spec - 1 do RMSE_sum = RMSE_sum $
            + (log_CEF_arr(i) - (A + B*alog10(CI_arr(y,i))))^2 $
            + p*B2*(((noise2/width_mw1(y)) * imr1(y,i)) $
            + ((noise2/width_mw2(y)) * imr2(y,i)))

current_RMSE = sqrt(RMSE_sum/n_spec)

if z eq 0 then begin
      if y eq 0 then begin
            RMSE = current_RMSE
            print,'     ---'
            print,'Initial RMSE is',RMSE
            print,'Initial MW boundaries are',$
                  locmin_mw1_u,locmin_mw1_l,locmin_mw2_u,locmin_mw2_l
            print,'     ---'
      endif
endif

      if y gt 0 then begin

            n_pot = n_pot + 1

;This signifies that one additional attempt has been made at changing the
MW bounds

            prob = exp(-(current_RMSE - RMSE) / (const * T))

;This is the probability of accepting this particular change. The change
is accepted if a random number between 0 and 1 is less than it (this has
the same probability of occurrence as 'prob').

      print,'Probability of acceptance is',prob
            if randomu(seed_2) lt prob then begin
                  print,'Accepted'
                  RMSE = current_RMSE
                  print,'New RMSE is',RMSE
                  n_acc = n_acc + 1
                  if y eq 8 then det = 0 else det = y + 1
                  z = 1
```

```
case y of

      1: locmin_mw1_u = locmin_mw1_u + step_size
      2: locmin_mw1_u = locmin_mw1_u - step_size
      3: locmin_mw1_l = locmin_mw1_l + step_size
      4: locmin_mw1_l = locmin_mw1_l - step_size
      5: locmin_mw2_u = locmin_mw2_u + step_size
      6: locmin_mw2_u = locmin_mw2_u - step_size
      7: locmin_mw2_l = locmin_mw2_l + step_size
      8: locmin_mw2_l = locmin_mw2_l - step_size

endcase

      print,'New MW boundaries are',$
      locmin_mw1_u,locmin_mw1_l,locmin_mw2_u,locmin_mw2_l

      de = 0
      x = 0
      break

      endif else begin
            if y eq 8 then det = 0 else det = y + 1
            print, 'Rejected'
            print, '     ---'
            de = de + 1
      if det eq 0 then begin
            if de lt 8 then begin
                  x = 0
                  break
            endif
      endif
      endelse

endif

endfor

;If a 'break' has occurred, the program escapes from the 'for' loop and
returns to the 'while' loop. If it does not, then the program will end at
the end of the for loop as x was set to 1 (ie while loop unsatisfied) at
the beginning of the while loop. The break will only fail to occur after
8 consecutive rejections of the newly presented MW boundaries.

z = 1

endwhile

end
```

Appendix 4.8: Simulated Annealing - MW centres and widths varied

```
;Define the middle values of the two MWs

mmw1 = (784.5 - 685)*40
mmw2 = (819.5 - 685)*40

;Define the width of the two MWs

width1 = 20
width2 = 20

;Define spectral arrays

th_arrstr = ['06000','09000','12000','15000','18000','21000']
th_arr = [6,9,12,15,18,21]
;Tangent height

atm_arr =
['ngt','equ','win','sum','ngt_var','equ_var','win_var','sum_var']
;Atmosphere type

kext_arrstr = ['0.001','0.01','0.1']
kext_arr = [0.001,0.01,0.1]
;Extinction coefficient

CT_arrstr = ['-2.0','-1.5','-1.0','-0.5','0.0','0.5','1.0','1.5','2.0']
CT_arr = [-2.0,-1.5,-1.0,-0.5,0,0.5,1.0,1.5,2.0]
;Displacement of cloud top from tangent height

n_spec =
n_elements(th_arrstr)*n_elements(atm_arr)*n_elements(kext_arrstr)*n_eleme
nts(CT_arrstr)

CI_arr = dblarr(n_spec)

meanrad1 = dblarr(n_spec)
meanrad2 = dblarr(n_spec)

p = 1/alog(10)^2

lad_arr = fltarr(2)

x = 0
z = 0

noise2 = 25.0 ^ 2

restore,'logCEF.sav'

det = 0         ;These have the same function as before
T = 2
const = 0.005
n_pot = 0
n_acc = 0

seed1 = 111111
```

```
seed2 = 111112
seed3 = 111113
seed4 = 111114
seed5 = 111115
seed6 = 111116
seed7 = 111117

de = 0

while x eq 0 do begin

if z gt 0 then begin

mmw1 = mmw1 + fix((randomu(seed1) - 0.5) * 5 * T + 0.5)
mmw2 = mmw2 + fix((randomu(seed2) - 0.5) * 5 * T + 0.5)

width1 = width1 + fix((randomu(seed3) - 0.5) * 5 * T + 0.5)
width2 = width2 + fix((randomu(seed4) - 0.5) * 5 * T + 0.5)

;These determine the magnitude of the changes to the middle position of
the MWs and the width, respectively. Both are dependant on T.

if width1 lt 1 then width1 = 1
if width2 lt 1 then width2 = 1

endif

locmin_mw1_u = mmw1 + width1
locmin_mw1_l = mmw1 - width1
locmin_mw2_u = mmw2 + width2
locmin_mw2_l = mmw2 - width2
;These are the upper and lower bounds of the 2 MWs

x = 1

if n_pot eq 15 then begin
   T = T * 0.9
   n_pot = 0
   n_acc = 0
endif

if n_acc eq 7 then begin
   T = T * 0.9
   n_pot = 0
   n_acc = 0
endif

print,'     ---'
print,'T is',T

index = 0

;Load in the spectra.

for l = 0,n_elements(th_arr)-1 do begin
      for k = 0,n_elements(kext_arr)-1 do begin
            for j = 0,n_elements(CT_arr)-1 do begin
                  for i = 0,n_elements(atm_arr)-1 do begin
```

```
if CT_arr(j) ne -2.0 then begin

      str =
      atm_arr(i)+'_'+CT_arrstr(j)+'_'+kext_arrstr(k)+'_'+th_arrstr(l)

      rfmrd,'/home/jupiter/eodg/hurley/janeRFM$
      /rad_cloudy_CFCs_'+str+'.asc',W,r

endif else begin

      str = atm_arr(i)+'_nopert'+th_arrstr(l)

      rfmrd,'/home/jupiter/eodg/hurley/janeRFM$
      /rad_clearA_CFCs_'+str+'.asc',W,r

endelse

width_mw1 = locmin_mw1_u - locmin_mw1_l + 1
width_mw2 = locmin_mw2_u - locmin_mw2_l + 1

meanrad1(index) = mean(r(locmin_mw1_l:locmin_mw1_u))
meanrad2(index) = mean(r(locmin_mw2_l:locmin_mw2_u))

CI_arr(index) = meanrad1(index) / meanrad2(index)

index = index + 1

endfor
endfor
endfor
endfor

imr1 = 1/meanrad1^2
imr2 = 1/meanrad2^2

      RMSE_sum = 0.0D0

      lad_arr(*) = ladfit(alog10(CI_arr(*)),log_CEF_arr(*))

      A = lad_arr(0)
      B = lad_arr(1)
      B2 = B^2

      for i = 0,n_spec - 1 do RMSE_sum = RMSE_sum $
            + (log_CEF_arr(i) - (A + B*alog10(CI_arr(i))))^2 $
            + p*B2*(((noise2/width_mw1) * imr1(i))$
            + ((noise2/width_mw2) * imr2(i)))

current_RMSE = sqrt(RMSE_sum/n_spec)

if z eq 0 then begin
   RMSE = current_RMSE
   print,'Initial RMSE is',RMSE
   x = 0
endif

n_pot = n_pot + 1
```

```
if z gt 0 then begin
      prob = exp(-(current_RMSE - RMSE) / (const * T))

      print,'Probability of acceptance is',prob
            if randomu(seed7) lt prob then begin
                  print,'Accepted'
                  RMSE = current_RMSE
                  print,'New RMSE is',RMSE
                  n_acc = n_acc + 1
                  x = 0

      print,'New MW boundaries are',$
      locmin_mw1_u,locmin_mw1_l,locmin_mw2_u,locmin_mw2_l

      de = 0

      endif else begin
            print, 'Rejected'
            print, '     ---'
            de = de + 1
            if de lt 6 then x = 0
      endelse

endif

z = 1

endwhile

end
```

Appendix 4.9: Calculation of number of clear spectra lost given threshold at maximum cloudy CI, for each 1 wide MW combination

```
restore,'Smooth_Results.sav'
;This gives meanrad1 (81225,1296), meanrad2 (81225,1296), and alt (1296).

;CI_noise stores the new CI values, with noise added for cloudy ones and
subtracted for clear ones, as a first approximation of the noise
contribution. All the current mws are of width 40, so the number of
points in each is 41.

c = 25/sqrt(41) & c2 = c^2

threshold = fltarr(81225)
n_lost = fltarr(81225)
CI_noise = fltarr(81225,1296)

clear = where(alt eq -2.0)
n_clear_spectra = n_elements(clear)
cloudy = where(alt gt -2.0)
cloudy2 = where(alt gt -1.5)

;cloudy2 discounts (although not exclusively) the lowest rung of cloudy
spectra. It is used for the threshold calculation.

for i = 0L,81224 do begin

;Add the noise contribution to the cloudy spectra

     for j = 0,n_elements(cloudy) - 1 do begin

          noise = c2*(meanrad1(i,cloudy(j))^2/meanrad2(i,cloudy(j))^2)*$
          (1 / meanrad1(i,cloudy(j))^2 + 1 / meanrad2(i,cloudy(j))^2)

          CI_noise(i,cloudy(j)) = meanrad1(i,cloudy(j)) $
          / meanrad2(i,cloudy(j)) + noise

     endfor

;Subtract the noise contribution from the clear spectra.

     for j = 0,n_clear_spectra - 1 do begin

          noise = c2*(meanrad1(i,clear(j))^2 / meanrad2(i,clear(j))^2)*$
          (1 / meanrad1(i,clear(j))^2 + 1 / meanrad2(i,clear(j))^2)

          CI_noise(i,clear(j)) = meanrad1(i,clear(j))$
          / meanrad2(i,clear(j)) - noise

     endfor

     threshold(i) = max(CI_noise(i,cloudy2))
     n_lost(i) = n_elements(where(CI_noise(i,clear) le threshold(i)))

endfor
end
```

Appendix 4.10: Calculation of number of SDs between clear mean and cloudy threshold for width 1 MW combinations

```
restore,'Smooth_Results.sav'

;Create arrays which store the mean, SD and threshold for each MW
combination. Mean and SD are just for the clear spectra; threshold, as
before, is just for the cloudy spectra (excluding CTH of -1.5 and
including noise). 'Result' gives the number which we want to maximise.

c = 25/sqrt(41) & c2 = c^2

SD_arr = fltarr(81225)
mean = fltarr(81225)
threshold = fltarr(81225)

result = fltarr(81225)

cloudy2 = where(alt gt -1.5)
clear = where(alt eq -2.0)
n_clear_spectra = n_elements(clear)

CI_noise_cloudy = fltarr(81225,n_elements(cloudy2))

;CI_noise_cloudy stores the CI values for just the cloudy spectra, with
noise contribution added

for i = 0L,81224 do begin

      SD_sum = 0.0D0        ;Includes noise contribution
      mean_sum = 0.0D0      ;The sum of the clear spectrum CIs

      for j = 0,n_clear_spectra-1 do mean_sum = mean_sum + $
      meanrad1(i,clear(j)) / meanrad2(i,clear(j))

      mean(i) = mean_sum / n_clear_spectra

      for k = 0,n_clear_spectra-1 do SD_sum = SD_sum +
      (meanrad1(i,clear(k)) / meanrad2(i,clear(k)) $
      - mean(i)) ^ 2 + (c2 * (meanrad1(i,clear(k))^2 / $
      meanrad2(i,clear(k))^2) * $
      (1 / meanrad1(i,clear(k))^2 + 1 / meanrad2(i,clear(k))^2))

;The second term in the above sum is the noise contribution.

      SD_arr(i) = sqrt(SD_sum / n_clear_spectra)

      for l = 0,n_elements(cloudy2) - 1 do begin

            noise = c2 * (meanrad1(i,cloudy2(l))^2 / $
            meanrad2(i,cloudy2(l))^2) * $
            (1 / meanrad1(i,cloudy2(l))^2 + 1 / meanrad2(i,cloudy2(l))^2)

            CI_noise_cloudy(i,l) = meanrad1(i,cloudy2(l)) / $
            meanrad2(i,cloudy2(l)) + noise

      endfor
```

```
      threshold(i) = max(CI_noise_cloudy(i,*))
      result(i) = (mean(i) - threshold(i)) / SD_arr(i)
      print,i

endfor

save,result,threshold,SD_arr,mean,filename = 'SD_thresholds.sav'

end
```

Appendix 4.11: Calculation of ratio of mean difference to SD sum for each width 1 MW combination

```
restore,'Smooth_Results.sav'
;This gives meanrad1 (81225,1296), meanrad2(81225,1296), and alt (1296),
which expresses the cloud top height relative to the tangent height.

restore,'Reference2.sav'
;This gives ext (storing extinction coefficient values), amongst other
arrays.

;Now we also want mean_cloudy and SD_cloudy for each MW combination.
Result is modified. There is no longer any 'threshold'. Want the mean and
SD for all cloudy spectra except those with CTH of -1.5 and ext of 0.001.

c = 25/sqrt(41) & c2 = c^2

SD_clear = fltarr(81225)
mean_clear = fltarr(81225)
mean_cloudy = fltarr(81225)
SD_cloudy = fltarr(81225)
result2 = fltarr(81225)

clear2 = where(alt eq -1.5 and ext eq 0.001)

cloudy = fltarr(1104)
n_poor_cloud = n_elements(cloudy)

clear = where(alt eq -2.0)
n_clear_spectra = n_elements(clear)

index = 0

for i = 0,1295 do begin

      change = 1

      for j = 0,n_clear_spectra - 1 do begin

            if i eq clear(j) then change = 0

      endfor

      for k = 0,n_elements(clear2) - 1 do begin

            if i eq clear2(k) then change = 0

      endfor

      if change then begin

            cloudy(index) = i
            index = index + 1

      endif

endfor
```

```
;This populates the array 'cloudy' with the appropriate element numbers
of the 1296 spectra.

for i = 0L,81224 do begin

      mean_clear_sum = 0.0D0
      SD_clear_sum = 0.0D0
      mean_cloudy_sum = 0.0D0
      SD_cloudy_sum = 0.0D0

;Calculate mean of clear spectral CIs

      for j = 0,n_clear_spectra - 1 do mean_clear_sum = mean_clear_sum +$
           meanrad1(i,clear(j)) / meanrad2(i,clear(j))

      mean_clear(i) = mean_clear_sum / n_clear_spectra

;Calculate SD of clear spectral CIs

      for k = 0,n_clear_spectra - 1 do SD_clear_sum = SD_clear_sum + $
           (meanrad1(i,clear(k))/meanrad2(i,clear(k))-mean_clear(i))^2+$
           (c2 * (meanrad1(i,clear(k))^2 / meanrad2(i,clear(k))^2) * $
           (1 / meanrad1(i,clear(k))^2 + 1 / meanrad2(i,clear(k))^2))

      SD_clear(i) = sqrt(SD_clear_sum / n_clear_spectra)

;Calculate mean of 'cloudy' spectral CIs

      for l = 0,n_poor_cloud - 1 do mean_cloudy_sum = mean_cloudy_sum + $
           meanrad1(i,cloudy(l)) / meanrad2(i,cloudy(l))

      mean_cloudy(i) = mean_cloudy_sum / n_poor_cloud

;Calculate SD of 'cloudy' spectral CIs

      for m = 0,n_poor_cloud - 1 do SD_cloudy_sum = SD_cloudy_sum + $
           (meanrad1(i,cloudy(m)) / meanrad2(i,cloudy(m)) $
           - mean_cloudy(m)) ^ 2 + $
           (c2 * (meanrad1(i,cloudy(m))^2 / meanrad2(i,cloudy(m))^2) * $
           (1 / meanrad1(i,cloudy(m))^2 + 1 / meanrad2(i,cloudy(m))^2))

      SD_cloudy(i) = sqrt(SD_cloudy_sum / n_poor_cloud)

;Calculate the desired ratio

      result2(i) = (mean_clear(i) - mean_cloudy(i)) / (SD_clear(i) + $
      SD_cloudy(i))

      print,i,result2(i)

endfor

save,result2,SD_clear,mean_clear,mean_cloudy,SD_cloudy,filename =
'SD_double.sav'
save,cloudy,filename = 'Cloudy.sav'

end
```

10. Bibliography

[1] Raspollini, Piera et al, 'Overview of MIPAS Operational Products', 2007
http://www.leos.le.ac.uk/publications/pdfs/jjr/463621pr_REV2.pdf

[2] Hurley, Jane, 'First Year Report: Modelling Clouds in the Infrared', August 2006, Exeter College, University of Oxford

[3] Piccolo, Chiara and Anu Dudhia, 'Precision Validation of MIPAS-ENVISAT Products', February 2007, Proceedings of the Third Workshop on the Atmospheric Chemistry Validation of Envisat (ACVE-3) 4-7 2006, ESRIN, Frascati, Italy

[4] Yiu, Ho-Ching Iris, 'Direct Pressure Retrieval from MIPAS Spectra', 2005, St Hilda's College, University of Oxford, MPhys project report

[5] Bormann, Niels et al., 'Simulating infrared limb radiances from MIPAS in the ECMWF system',
http://www.ecmwf.int/newsevents/meetings/workshops/2004/Assmilation_HSRS/Presentations/Bormann.pdf

[6] Robinson, Jim, 'CIO infrared emission spectrum retrieval using the Michelson Interferometer for Passive Atmospheric Sounding (MIPAS), April 2000,
http://www.atm.ox.ac.uk/group/mipas/reports/robinson.pdf

[7] Kaspryzyk, Dominik, 'Cloud Detection in MIPAS Spectra', April 2002
http://www.atm.ox.ac.uk/group/mipas/reports/kaspryzyk.pdf

[8] Rogers, P. R. and M. K. Yau, *A Short Course in Cloud Physics*, 1989, Pergamum Press, Oxford

[9] Borikov, A.M. et al, *Cloud Physics*, 1963, GIMIZ, Leningrad trans. S. Monson/Israel Program for Scientific Translation Ltd, Jerusalem

[10] Hurley, Jane, 'Second Year Report: Modelling Clouds in the Infrared', August 2007, Exeter College, University of Oxford, second year report submitted in partial fulfilment of DPhil

[11] Fletcher, Ben, 'Carbon Monoxide Retrievals from MIPAS', 2002,
http://www.atm.ox.ac.uk/group/mipas/reports/fletcher.pdf

All diagrams except figure 3 generated using IDL at Oxford University by Harry Desmond

11. Acknowledgements

I would like to thank Dr Anu Dudhia of the Department of Atmospheric, Oceanic and Planetary Physics, Oxford University for guidance and advice on this project, and also Jane Hurley of the same department for her help.